Article

Assessment of the Impact of Selected Parameters of Tractor-Semitrailer Set on the Braking Safety Indicators

Paweł Radzajewski [1] and Marek Guzek [2,*]

1 Pronar Ltd., 17-210 Białystok, Poland; radzajewskilech@wp.pl
2 Faculty of Transport, Warsaw University of Technology, 00-662 Warsaw, Poland
* Correspondence: marek.guzek@pw.edu.pl

Abstract: With the continuous development of road transport of goods, the issue of safety risks related to the movement of trucks and road trains remains an essential element of the overall road safety system. One of the persistent problems is the braking of such kits, especially in emergencies on the road. The work aims to show how typical changes in operating conditions can affect the basic indicators illustrating the safety of braking (effectiveness indicators, stability symptoms). A simulation method was applied for the analysis, which used a relatively simple (quasi-static) model of the tractor-semitrailer set's rectilinear motion and models of the braking system and the longitudinal forces in the tyre-road surface contact. Calculations were made for the selected truck-trailer set in nominal condition and for several deviations from the nominal state, such as loading the trailer (load value, location of the semi-trailer's centre of gravity), reduced surface adhesion, and selected faults of the semitrailer braking system. The results were compared for several qualitative and quantitative criteria for the evaluation of braking safety. Attention was drawn to the problem of the forces in the coupling (which determine the possibility of jack-knifing phenomena), the order of axle locking, and the braking distance. The presented results show that the change of operating conditions as above compared to the nominal condition visibly deteriorates the effectiveness of the braking process. The greatest threat, both related to the braking efficiency and the increase in the force in the coupling, is associated with the lack of braking of the semitrailer axle or a significant reduction in its load. The weight and location of the load's centre of gravity considerably impact braking safety. In addition to the negative impact on the braking distance or increase in the horizontal force in the coupling, it changes the order of locking the axle. ABS reduces the risk associated with braking safety but does not eliminate it. At the same time, it has been shown that using relatively simple calculation tools makes it possible to indicate the risks related to the braking safety of such articulated vehicles.

Keywords: safety of motor vehicle braking; simulation method; braking the tractor-semitrailer vehicle set; motor vehicle dynamics; trucks; articulated vehicle

1. Introduction

Road transport is the primary way of moving goods and people, and its share in the general transport market is constantly growing, which is evident in the statistics, e.g., [1,2]. If we limit ourselves to transporting goods only, in 2010, the transport performance in the EU-27 amounted to a total of approx. 3036 billion tkm, including the share of road transport amounted to 51%. In 2019 the total transport performance increased to 3392 billion tkm with the percentage of road transport at 52% [2]. In some countries, the dominance of road transport is even more pronounced (e.g., in Poland, the share of road transport in the amount of transport performance increased in 2010–2020 from approx. 70% to 85% [1]).

The increase in the transport of goods translates into an increase in the number of vehicles travelling on the roads. In the EU-27 countries, approx. 283 million motor vehicles are registered (2021), including approx. 35.6 million trucks. The number of motor vehicles

is systematically increasing. From 2010 to 2017, the number of freight vehicles increased by 9% [2].

The increase in road transport is one of the essential factors affecting safety. Although statistical data show a systematic reduction in road incidents, it is nevertheless the most dangerous type of transport. In the European Union, in 2021, the number of fatalities in road accidents amounted to 19.8 thousand [3–5]. As indicated by various studies on traffic safety, the main causes of accidents lie in the operators (drivers) of vehicles [3,6,7] and much less in the remaining elements of the transport system: human-vehicle-environment. Nevertheless, they are negligible in an analysis of road traffic safety. During vehicle inspections by the Polish Road Transport Inspection, as many as 4% of the tested vehicles showed malfunctions of the braking system, and 2% related to tyres, wheels and axles [8]. These were the most frequently detected faults in heavy goods vehicles.

The authors' area of interest is the vehicle. Therefore, further considerations will be limited to this element of the system. A vehicle with safety-appropriate characteristics contributes to a higher level of road safety. Commercial vehicles (lorries) play a specific role in this aspect. On the one hand, police reports show that only a few percent of the perpetrators of road accidents are drivers of trucks with a maximum permissible weight (GVW) above 3.5 t (e.g., in Poland in 2021, out of a total of 23,000 accidents, it is only approx. 3.3% of such events [5]). However, on the other hand, due to the general incompatibility of such vehicles with other means of road transport in terms of geometric, mass, and stiffness [6,9–13], the effects of road incidents involving such vehicles are much more significant. Analysing the data in [5], it can be seen that the severity of such accidents is much higher—15 deaths per 100 accidents, while the overall average for road accidents was 8.8. Another aspect of truck accidents is the potentially significantly higher material costs associated with the extent of infrastructure damage, vehicle damage, and cargo loss.

The driver's basic behaviour in emergencies is to brake the vehicle. Therefore, the course of the braking process and its impact on the vehicle's behaviour on the road is crucial for its active safety. The main areas of interest of scientists dealing with the braking safety of various vehicles are the impact of vehicle speed and mass [14–18] and the position of the centre of gravity [19,20] on deceleration and braking distance. Another discussed topic is the deceleration rise time [21]. The debated issue is also the impact of the design features of the braking system on its reaction time and directional stability of motion [22] or the effect of the lack of braking of the trailer [23,24] on the braking process of the set of vehicles as well as the experimental verification of numerical models, e.g., [25].

Vehicle stability is an essential aspect of such a process. It is affected, apart from the values of the braking forces and the state of wheel rotation movement (locked or not), by the distribution of these forces on the sides of the vehicle and individual axles. Improper ones can lead to loss of vehicle stability. This problem becomes particularly important in the case of vehicle combinations (lorry-trailer or road tractor-semitrailer). Here, such an improper distribution of forces on individual axles of vehicles, apart from the classic (described in the theory of motor vehicle motion, e.g., [26–28]) situation of the tendency for the vehicle to rotate in the road plane), may lead to the phenomenon of "jack-knifing", which results in the loss of control over the vehicle and a high risk of an accident (even though, for example, the braking efficiency indicators are good). To reduce the risk of such situations, vehicle braking systems must meet specific requirements formulated in normative acts, e.g., [29]. Among other things, they impose specific boundary characteristics of the distribution of braking forces for different categories of vehicles (this will be described in more detail in Section 3.2). However, these limitations cannot always protect a vehicle or a set of vehicles against the described threats in actual operating conditions. Wear and tear of vehicle components, changes in load, motion resistances, state of the road surface (its adhesion), etc., affect the actual indexes of utilised adhesion for individual axles.

Essential issues are time delays and times of increasing braking forces on vehicle wheels. They are the subject of research presented, for example, in [15,30–32]. According to the requirements of ECE [29], the reaction time of the braking system is understood as

the time elapsing from the moment of starting the actuation of the control device until the moment when the braking force of the most unfavourably located brake reaches the level corresponding to the required efficiency. In motor vehicles equipped with a service braking system wholly or partially dependent on an energy source other than the driver's muscular energy, the braking system's response time during emergency braking shall not exceed 0.6 s. In the case of towed vehicles, the braking system's response time measured without a motor vehicle should not exceed 0.4 s [29]. Excessive time delay in braking the towed vehicle can increase force in the coupling acting on the towing vehicle, consequently leading to a "jack-knifing" phenomenon.

Another important aspect in analysing safety and stability during braking is the tyres' adhesion to the road surface. It directly impacts the vehicle's behaviour (wheel locking, force distribution, motion stability, braking ratio). The characteristics of the unit tangential force in the contact tyre-road surface are influenced by the properties of the tyre (shape, tread type, wear, pressure, stiffness, compound type, year of production—age/age of the material) and the road surface (surface type, roughness, wear, weather conditions: the thickness of the layer of water, snow, ice cover etc.). This issue is the subject of many studies, e.g., the impact of the type of road surface [33–36], weather conditions [35,37–39], aerodynamic drag [40], tyre type and pressure [34,35,41,42], vehicle speed [33] or load [42]. Comparisons of simulation and experimental studies in the unit tangential forces, also taking into account lateral slip, can be found, for example, in [33,43–45]. Interesting work is [37], where authors propose an integrated tyre-vehicle model to evaluate vehicle braking performance based on Persson's friction theory. The topic of modelling contact forces will be mentioned in Section 2.2.

Tests for vehicles of a similar form to those considered in this article (trucks, articulated vehicles) can be found in the previously mentioned [17,39,40]. In paper [46], a three-dimensional model of a truck is proposed, but the research concerns fuel consumption in the context of road unevenness. The paper [47] proposes a methodology for simulation durability tests of vehicles and their assemblies. In both of these works, the unevenness of the road surface plays an important role. In paper [48] a numerical model was used to simulate the handling stability of a heavy tractor semi-trailer under Crosswind. Other works presenting the use of models to simulate the braking of trucks, e.g., such as V-sim, can be found in [49,50]. It is worth noting that most of the work on vehicle braking focuses on passenger cars, light commercial vehicles or prototype vehicles, both regarding braking dynamics and related topics (modelling tires—trucks, testing forces in the coupling). A limited number of available publications on heavy road vehicle assemblies in the issues mentioned above and road incidents suggest its topicality.

The literature review shows the multiplicity and diversity of research related to various aspects of motor vehicle braking and their topicality. The authors of this study are interested in the subject of efficiency and stability during the braking of the articulated vehicle in the form of a tractor and semitrailer. This article aims to present a relatively simple methodology that enables the assessment of the primary braking safety indicators of the vehicles set (braking distance, braking deceleration, braking time) and the quantities indicating the risk of loss of stability (wheel locking tendencies, force in the coupling). A simulation model of the braking of a tractor-semitrailer set will be presented, as well as calculations and their analysis in terms of the influence of selected factors (set configuration, loading, location of the centre of mass of the semi-trailer, road surface condition). Conducting tests using simulation methods is a justified form of research here (experimental tests are associated with high costs and risks to people and property). Such a research method will allow for a quick qualitative assessment of the scope of the motion safety of a tractor unit with a semi-trailer (or a truck with a trailer) in a wide range of changes in operating conditions. A quantitative assessment will also be possible if the simulation method is positively verified.

2. Materials and Methods

As mentioned, the topic under consideration is the braking of the tractor with a semitrailer (or, more generally, a set of towing and towed vehicles). The simulation method was adopted as the method of analysis. A functional diagram illustrating it is shown in Figure 1. The basic element is the model of the braking dynamics of the set of two vehicles and the models of essential subsystems—the pneumatic braking system, the ABS regulator and the tyre-road contact force model. A relatively simple model of the motion of a set of vehicles has been proposed. With determined technical parameters describing the towing and towed vehicle, defined initial conditions (speed) and the assumed action of the motor vehicle operator (e.g., the driver), it is possible to obtain time histories of forces and quantities describing the motion of the vehicles set for a specific operational state, i.e., set configuration, load and its distribution, adhesion of the tyres on the road surface or brake system faults. This, in turn, makes it possible to evaluate the safety of the analysed braking process in terms of its effectiveness and threats from the point of view of the vehicles set motion stability. In the following subsections, the individual elements of the described method are brought closer.
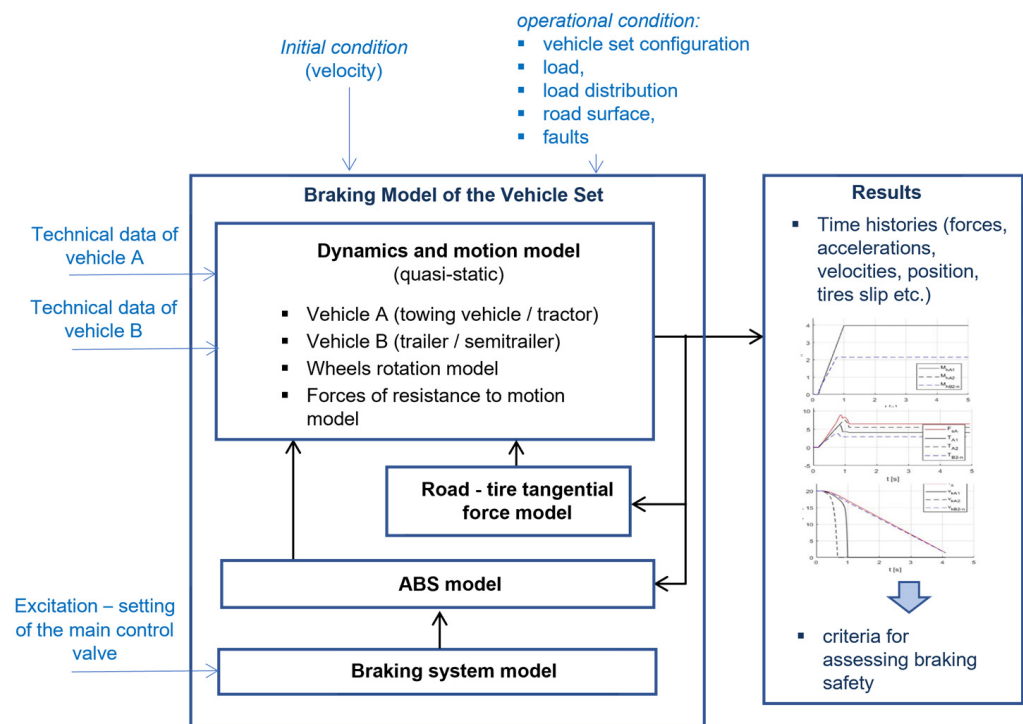

Figure 1. Functional diagram of the proposed research method.

2.1. Motion and Dynamics Model of a Set of Vehicles

Considered (Figure 2) is the translational motion of rigid bodies illustrating set elements: vehicle A (tractor) and vehicle B (semitrailer) in the vertical plane (*Oxz* coordinate system related to the road, horizontal *x*-axis, vertical *z*-axis), on a horizontal, even road surface. Alternatively, the vehicles set can be a truck with a trailer). The model assumes a rectilinear motion of the set along the *x*-axis. The movement of the masses of the set in the *z* direction is omitted, so the deflections of the suspension and tyres are not considered. The bodies of the set are modelled as a system of concentrated masses connected with weightless beams. They are subject to a flat system of forces. The motion resistances of the air drag force of the towing and towed vehicle (omitting wind speed) and rolling resistance forces of vehicle wheels are considered. The coupling model assumes the interaction of forces in two directions (*x*, *z*). The relative movements of vehicles are omitted (rigid articulated connection). Multiple (complex) axles are described with a single equivalent axle where the reactions acting on a single axle are

replaced by a sum of forces concentrated in the centre of the equivalent axle. The equivalent axle's position corresponds to the axles set geometric centre.
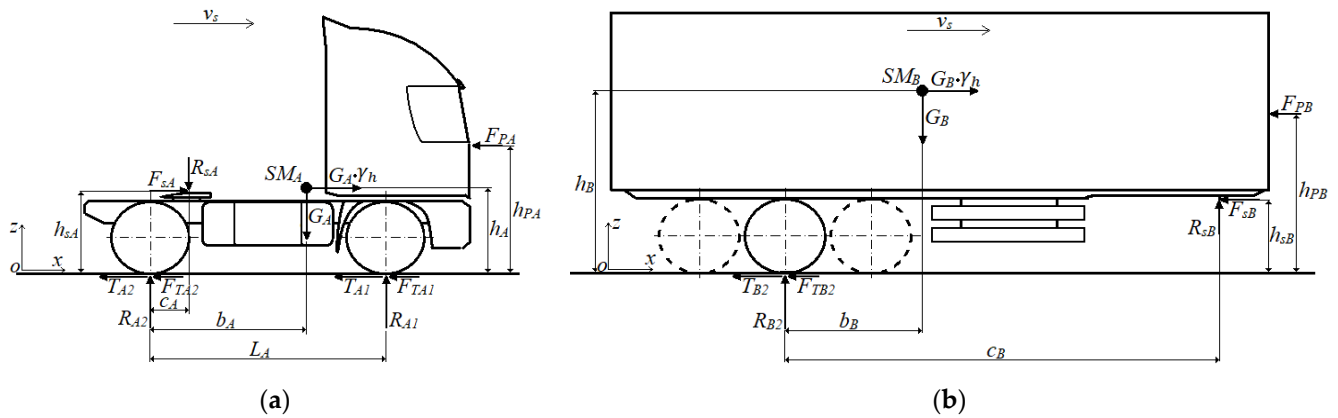

Figure 2. Physical model: (**a**) Forces acting on vehicle A (tractor); (**b**) Forces acting on vehicle B (semitrailer).

The quasistatic equilibrium equations for vehicle A have the following form:

$$\sum F_x = -T_{A1} - T_{A2} + G_A \cdot \gamma_h + F_{sA} - F_{PA} - F_{TA1} - F_{TA2} = 0 \tag{1}$$

$$\sum F_z = R_{A1} + R_{A2} - G_A - R_{sA} = 0 \tag{2}$$

$$\sum M_1 = G_A(L_A - b_A) - G_A \cdot \gamma_h \cdot h_A - R_{A2} \cdot L_A + R_{sA}(L_A - c_A) - F_{sA} \cdot h_s + F_{PA} \cdot h_{PA} = 0 \tag{3}$$

and for vehicle B:

$$\sum F_x = -T_{B2} + G_B \cdot \gamma_h - F_{sB} - F_{PB} - F_{TB2} = 0 \tag{4}$$

$$\sum F_z = R_{B2} - G_B + R_{sB} = 0 \tag{5}$$

$$\sum M_2 = -G_B \cdot \gamma_h \cdot h_B - G_B \cdot b_B + R_{sB} \cdot c_B + F_{sB} \cdot h_s + F_{PB} \cdot h_{PB} = 0 \tag{6}$$

The symbols used in Figure 2 and the above formulas mean: SM—vehicle centre of mass, L—wheelbase, h—height of the vehicle's centre of mass above the ground, b—distance of the vehicle's centre of mass from the vertical plane passing through the rear axle, h_s—height of the coupling (fifth-wheel) position above the ground, c—distance of the coupling position from the vertical plane passing through the rear axle, h_P—height above the ground of the resultant force of air drag.

Symbols T denote braking forces, G—vehicle weight, R—normal ground reactions, and F—forces of resistance to motion: F_P—air drag force, F_T—rolling resistance forces.

Index A indicates the values for the towing vehicle (A), and index B—for the towed vehicle (B). Indexes 1, 2—consecutive axles of the vehicle (front and rear, respectively).

The quantity γ_h appearing in the dependencies is the braking intensity (braking ratio) ([26–29,51]):

$$\gamma_h = \frac{-(m_A + m_B) \cdot \ddot{x}_s}{G_A + G_B} = \frac{-\ddot{x}_s}{g} = \frac{-\dot{v}_s}{g} \tag{7}$$

where: $m_{A/B}$—mass of vehicle A/B, v_s—vehicle velocity, g—acceleration of gravity, $\ddot{x}_s$—vehicle acceleration.

The equilibrium conditions for the coupling of *A* and *B* vehicles can be written as follows:

$$F_{sA} = F_{sB} = G_B \cdot \gamma_h - T_{B2} - F_{PB} - F_{TB2} \tag{8}$$

$$R_{sA} = R_{sB} = G_B - R_{B2} \tag{9}$$

Dependencies (8) and (9) combine Equations (1)–(3), (5) and (6), i.e., the tractor and semitrailer model. For a given velocity v_s and its derivative, the following forces are known: gravity G_A, G_B, resistance to motion F_{TA1}, F_{TA2}, F_{TB2}, F_{pA}, F_{pB}, tyre-road contact forces T_{A1}, T_{A2}, T_{B2}. It makes it possible to determine the tangential and vertical forces in the coupling $F_{sA} = F_{sB}$, $R_{sA} = R_{sB}$. The normal vertical reactions acting on the tractor and trailer axles are unknown: R_{A1}, R_{A2}, R_{B2}. The solution of the system of Equations (1)–(3), taking into account (8) and (9), leads to the dependence of these reactions:

$$R_{A1} = G_A \cdot \left(\frac{b_A}{L_A} + \frac{h_A}{L_A} \cdot \gamma_h \right) + R_{sA} \frac{c_A}{L_A} + F_{sA} \cdot \frac{h_s}{L_A} - F_{PA} \cdot \frac{h_{PA}}{L_A} \tag{10}$$

$$R_{A2} = G_A \cdot \left(1 - \frac{b_A}{L_A} - \frac{h_A}{L_A} \cdot \gamma_h \right) + R_{sA} \left(1 - \frac{c_A}{L_A} \right) - F_{sA} \cdot \frac{h_s}{L_A} + F_{PA} \cdot \frac{h_{PA}}{L_A} \tag{11}$$

$$R_{B2} = G_B \cdot \left(1 - \frac{b_B}{c_B} - \frac{h_B - h_s}{c_B} \cdot \gamma_h \right) - T_{B2} \cdot \frac{h_s}{c_B} + F_{PB} \cdot \frac{h_{PB} - h_s}{c_B} - F_{TB2} \cdot \frac{h_s}{c_B} \tag{12}$$

The rotary motion of the wheels is taken into account. Two road wheels of an axle are treated as one substitute wheel. The model of the wheel rotation is presented in Figure 3. The equation of the equilibrium of moments is as follows:

$$\sum M = -T_i \cdot r_{di} + M_{Hi} - M_{bki} + R_i \cdot e_i = 0 \tag{13}$$

where: r_d—dynamic radius of tyre, e—shift of the resultant vertical reaction acting on the wheel, T—tangential force in the tyre-road contact, M_H—given wheel braking moment, M_{bk}—moment of inertia acting on the wheel, $M_{bk} = -I_k \cdot \dot{\omega}_k$, I_k—a mass moment of inertia of the wheel.
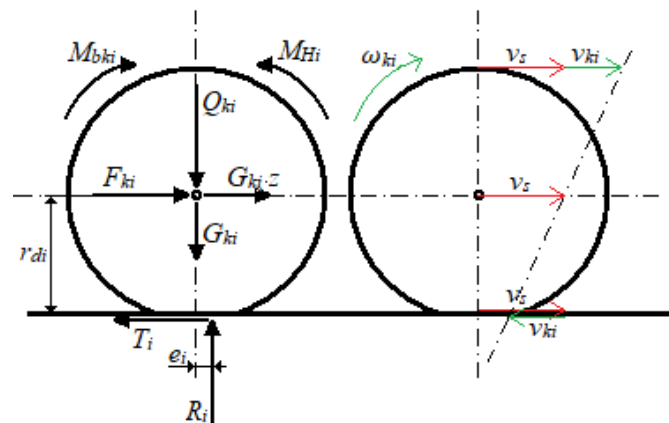
Figure 3. Diagram of forces and moments acting on a wheel and quantities describing its kinematic state (description in the text).

The index "*i*" denotes a given axle of the vehicles set (*i* = *A*1, *A*2, *B*2*n*), where "*n*" stands for the number of a single axle in the ensemble axles.

Equation (13) can be written in the form of a balance of forces:

$$-T_i + F_{Hi} + \frac{I_{ki}}{r_{di}} \cdot \dot{\omega}_{ki} + F_{Ti} = 0 \tag{14}$$

where: $F_H = \frac{M_H}{r_d}$ is the given wheel braking force, and $F_T = R\frac{e}{r_d}$ is the rolling resistance force.

The values of the tyre-road contact forces result from the model of tyre-road surface contact (see Section 2.2). Braking forces result from the excitation in the form of a time course of the position angle of the main control valve adjuster in the braking system model, which results in the braking moments on the wheels of vehicles (see Section 2.3).

Rolling resistance force express rolling friction and energy losses related to tyre deformation [26–28,52]. The following formula can represent this force (see e.g., [26–28] and also Equation (14)):

$$F_{Ti} = f_{vi} \cdot R_i \text{ and } f_{vi} = f\left(1 + A_t v_{ki}^2\right) \tag{15}$$

where: f_v—rolling resistance coefficient, v_k—circumferential velocity of the wheel, coefficients f and A_t result from the properties of the tyre (structure, pressure) and the road surface (see [26–28]).

Air drag force expresses the aerodynamic drag acting against a vehicle in the opposite direction to its movement. Its description was adopted as in [26–28]:

$$\text{vehicle A}: \ F_{PA} = c_{xA} \cdot A_A \cdot \rho \frac{v_s^2}{2} \tag{16}$$

$$\text{vehicle B}: \ F_{PB} = \Delta c_x \cdot F_{PA} + c_{xB} \cdot \Delta A_B \cdot \rho \frac{v_s^2}{2} \tag{17}$$

where: c_{xA}—drag coefficient for vehicle A, A_A—reference area (the front area of the tractor), ρ—air density, Δc_x—the relative air drag coefficient for the towed vehicle (relative to the towing vehicle), c_{xB}—drag coefficient for vehicle B, ΔA_B—the cross-sectional area of the elements of the vehicle B projecting beyond the contour of the vehicle A.

In the calculations presented further, it is assumed that the points of application of F_P forces lie at half of the vehicle height.

The model in the form shown in Figure 2 (tractor-semitrailer set) has 4 degrees of freedom. Generalised coordinates are displacement of the set along the axis Ox—x_s and three wheel rotation angles φ_i (i = $A1$, $A2$, $B2$). From the equations of the balance of horizontal forces (1) and (13), the second derivatives are:

$$\ddot{x}_s = \dot{v}_s = -\frac{\sum T_i + \sum F_{op}}{G_A + G_B} \cdot g = -\frac{T_{A1} + T_{A2} + T_{B2} + F_{PA} + F_{PB} + F_{TA1} + F_{TA2} + F_{TB2}}{G_A + G_B} \cdot g \tag{18}$$

$$\ddot{\varphi}_i = \dot{\omega}_{ki} = (T_i - F_{hi} - F_{Ti})\frac{r_{di}}{I_{ki}}, \ i = A1, \ A2, \ B2 \tag{19}$$

The above system of differential equations is solved with the use of Matlab.

2.2. Tyre-Road Tangential Force Model

In the literature, we can find many models used in simulation studies of the dynamics of motor vehicles, describing the unit tangential force μ (ratio of the tangential force T to the normal reaction R) in the tyre-road contact. They differ in the area of application and the way of mapping contact forces. There are simple physical models as well as very complex models reflecting the actual structure of the tire and the surface cooperating with it [26,53–56]. An interesting proposal can be found in the mentioned work [37] where the authors present an integrated tire-vehicle model to evaluate vehicle braking performance based on Persson's friction theory with a tyre hydroplaning finite element (FE) model, and a vehicle dynamic analysis. The use of the FE method for tire modeling can also be found, for example, in [57,58] (the impact of thermal phenomena is considered here). The approach presented in [59] is also interesting, where, based on the third LuGree model, a fuzzy model for determining the adhesion coefficients is proposed. However, the most often, they are the so-called semi-empirical models such as Magic Formula [60], the model

of Dugoff, Fancher, Segel [61], the TM-Easy model [62] or UniTire [63]. They vary in the degree of complexity. The author's modification of the Burckhardt model [64,65] is used in the study presented here. The advantage of the classic Burckhardt model is a simple analytical form with a reasonable degree of accuracy and ease of modification [66]. Based on this model, a modified version was created better to reflect the unit tangential force in the tyre-road contact, depending on the normal force point and wheel axle velocity, and to adjust its characteristics to the experimental test results. The segment of Burckhardt's original formula containing the c_4 (see [64,65]) has been replaced with new coefficients. The unit longitudinal tangential force in contact of the wheel with the road surface is expressed as:

$$\mu(s) \ = \ \left[c_1\left(1 - e^{-s \cdot c_2}\right) - s \cdot c_3 \cdot G_p\right] \cdot G_s \cdot \left(1 - c_5 \cdot F_z^2\right) \tag{20}$$

The following formulas define the G_p and G_s coefficients:

$$G_p \ = \ \frac{e^{-c_{p3} \cdot v}}{c_{p2}} \tag{21}$$

$$G_s \ = \ c_{p1} \cdot v - 0.5 \cdot arctan\left(-c_{p4} \cdot s \cdot v\right) + 1 \tag{22}$$

where: c_1, c_2, c_3—set of coefficients depending on the road surface and the tyre (see [64,65]), c_5—the additional coefficient for the dependence of the unit tangential force on the normal force R, $c_{p1}, c_{p2}, c_{p3}, c_{p4}$—set of coefficients for the dependence on the vehicle speed, s—tyre slip ratio, v—vehicle speed.

The tyre slip ratio results from the wheel kinematic state (Figure 3). For the *i*-th wheel, it can be expressed as:

$$s_i \ = \ \frac{v_s - v_{ki}}{v_s}, \quad v_{ki} \ = \ \omega_{ki} \cdot r_{di} \tag{23}$$

The tangential force at the point of contact of the wheel of the *i*-th axis with the road surface can be written as:

$$T_i \ = \ \mu(s_i) \cdot R_i \tag{24}$$

2.3. Braking System Model and ABS Model

When modelling the braking system, the following were taken into account: braking axes (brake cylinders, actuating mechanism), averaged response time on pneumatic lines, trailer brake valve with adjustable predominance, LSV valve (Load Sensing Valve), relay valve, pressure reduction valve and pressure limiting valve.

Using the dependencies contained in [44], the braking torque of the wheel depending on the pressure at the entrance to the brake cylinder, we can write:

$$M_H \ = \ k \cdot \left(\left(A_s \cdot p_{(s)} - B_s\right) \cdot l - C_0\right) \cdot \eta \cdot BF \tag{25}$$

where: A_s, B_s—coefficients describing the equation of force on the brake cylinder piston rod depending on the pressure, $p_{(s)}$—pressure at the input to the brake cylinder, k—number of brake cylinders on the axis, l—effective length of the brake lever, C_0—minimum brake input torque, η—the efficiency of the brake mechanism, BF—Brake Factor (the ratio of the braking torque to the torque generated at the end of the actuator lever [44]).

The above parameters needed to calculate the braking torque of a wheel can be determined using experimental methods [67,68] or catalogue data [69,70].

A correctly designed braking system should ensure optimal distribution of braking forces for an unladen and laden vehicle. It guarantees braking performance (short braking distance) and directional stability during braking, which results in meeting the requirements of ECE regulations on braking systems [29]. If the constant distribution of braking forces does not meet these requirements for both loading conditions, it is necessary to install devices regulating the distribution of braking forces between the different axles of the

vehicles set depending on the load condition. The problem of the distribution of braking forces in the set considered in the study will be presented in Section 3.2.

The basic formula describing the relationship between the output value (pressure at the actuators of the braking axles) and the input value (the position angle of the main control valve adjuster α or pressure in the control coupling head p_m) in a pneumatic brake system can be written as:

$$p_{(s)} = i_{h1} \cdot (i_{h2} \cdot (\cdots \cdot (i_{zh} \cdot (\alpha - \alpha_0) - \ldots) - p_{02}) - p_{01}) \cdot i_r \qquad (26)$$

where: i_{zh}—slope of the linear characteristic of the main control valve, $i_{h1}, i_{h2}, \ldots$ —slope of the linear characteristic of the other valves (relay valves, reduction valve), i_r—coefficient describing the ratio of the output value to the input value pressure reducer, α_0—minimum angle at which the brakes are actuated ('idle stroke'), $p_{01}, p_{02}, \ldots$ —minimum pressure values needed to actuate the valve (positive value) or pressure values for valve with adjustable predominance (negative value).

The above Equation (26) is an example and depends on the model of a specific braking system. This notation makes it easier to add additional valves or not to include them (by replacing $i_{hx} = 1$ and $p_{0x} = 0$). In addition, it is possible to change the order of the valves without interfering with the mathematical record.

The complete model of the pneumatic braking system used for the presented calculations is more complex. It includes many conditional functions, e.g., maximum pressure (brake system maximum working pressure, axle pressure limiters), inability to obtain negative pressures or pressures greater than the supply pressure, which generates a linear mathematical record of pneumatic elements. Also, such functions are needed to describe valve with adjustable predominance, valves with linear-broken characteristics or lifting axle control valve. Additionally, the time delay of pressure $p_{(s)}$ and p_m on pneumatic lines is simulated by shifting the pressure increase with time.

An example of a simplified diagram of a pneumatic braking system with an ABS system corresponding to the model used in the presented work for a tractor is shown in Figure 4.
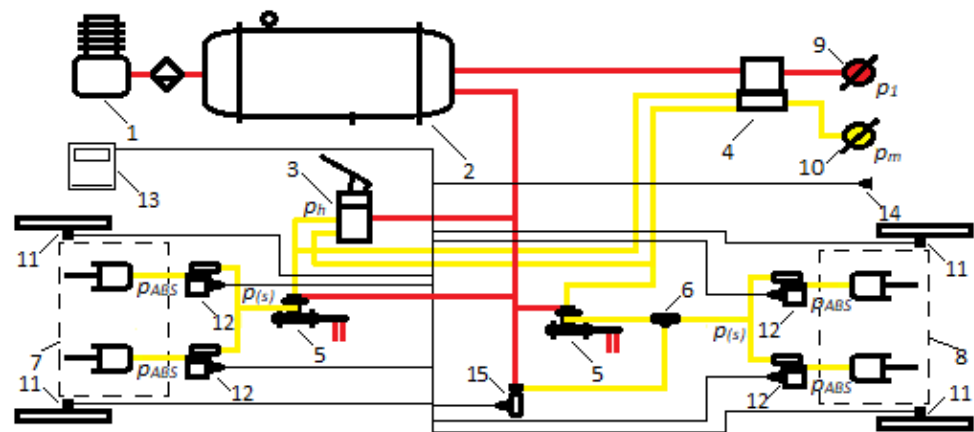
Figure 4. A simplified diagram of the pneumatic system of a towing vehicle equipped with ABS and ASR; 1—supply system, 2—air reservoir, 3—dual circuit foot brake valve with treadle actuation (main control valve adjuster), 4—trailer brake control valve, 5—Load Sensing Valve (LSV)—pneumatic, 6—two-way directional valve, 7—front axle brake actuators, 8—rear axle brake actuators, 9—supply coupling head, 10—control coupling head, 11—wheel speed sensor, 12—ABS modulator, 13—ABS controller, 14—trailer ABS control coupling head, 15—ASR valve.

The tyre-road contact force model is also enriched with a simple model of the anti-lock braking system ABS, in which the pressure hitting the brake cylinders of individual wheels is regulated by simulating ABS modulators. The ABS model detects changes in the

rotational speed of the wheels and the vehicle speed and limits the pressure at the output of the modulators, keeping the value of the relative slip s of a wheel close to $0.1 \div 0.3$. The idea of this model is illustrated on Figure 5. In the presented work, the ABS model is not the subject of research, so the authors wanted to create a simple, modifiable tool that would change the output signal from the brake system, reflecting the effect of the real ABS system. The input data are the values: s—relative longitudinal wheel slip, $p_{(S)}$—pressures input the brake cylinders when the ABS is turned off and constant parameters: s_{max}—slip ratio set as the maximum allowable—point 2 in Figure 5b, s_{min}—minimum slip ratio—point 3, s_{off}—slip value below which the ABS turns off—point 4, Δp_{ABS} i Δt_{ABS}—parameters describing the value and time of pressure drop or increase during the operation of the ABS modulator. If the slip ratio is higher than the maximum value (point 2), the ABS "controller" sends a signal to the modulator, which will decrease the pressure value (p_{ABS}), which goes to the brake cylinder. When the slip of a given wheel drops below the minimum value (point 3), the pressure controlled by the modulator reaching the brake cylinder starts to increase again in accordance with the adopted modulator parameters. Then the unit longitudinal force μ remains close to the maximum value—point 1. If the slip ratio drops below the adopted value corresponding to point 4, the ABS is deactivated and the pressure returns to the value resulting from the operation of the pneumatic braking system.
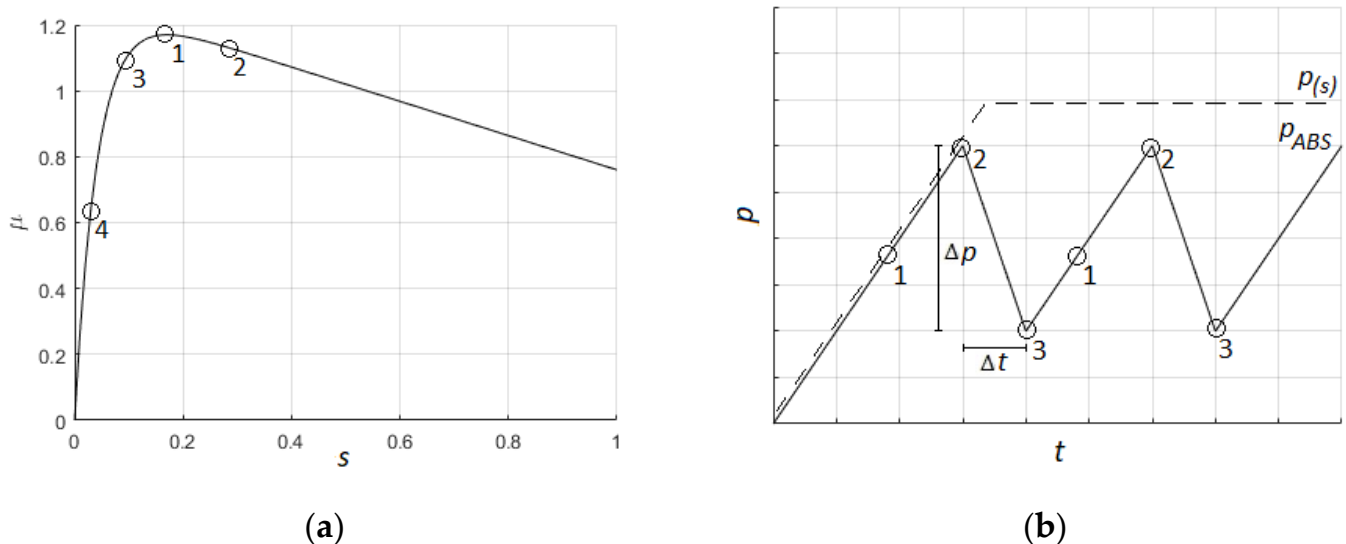
Figure 5. ABS operation diagrams: (**a**) Dependence of the adhesion coefficient on the slip ratio; (**b**) Change of pressure in the brake cylinder over time.

3. Results and Discussion

3.1. Considered Vehicle Sets and Braking Variants

Several typical cases reflecting the characteristic operating conditions describing the motion of a set of a tractor with a semitrailer were adopted for the research:

- b1: tractor + laden semitrailer, nominal set,
- b2: tractor + unladen semitrailer,
- b3r: tractor + laden semitrailer, with uneven load distribution—shifting the trailer's centre of gravity towards the rear,
- b3f: tractor + laden semitrailer, with uneven load distribution—shifting the trailer's centre of gravity towards the front,
- b4: tractor + laden semitrailer, with exceeded maximum permissible weight (GVW),
- b5: tractor + laden semitrailer, failure of the semitrailer braking system (brakes not working),
- b6: tractor + laden semitrailer, failure of the semitrailer braking system (longer reaction time),

- b7: tractor + laden semitrailer, surface with reduced adhesion (wet asphalt),
- b8: tractor + laden semitrailer, surface with reduced adhesion (icy road).

Table 1 presents the nominal values of the main parameters describing vehicles A and B (these data were adopted based on technical data of selected vehicles [71,72] and literature data [28,29,38,52,66,73].

Table 1. Technical data of vehicles.

Property	Vehicle A	Vehicle B	
wheelbase	$L_A = 3.65$ m		$L_B = 2.62$ m
mass	$m_A = 7395$ kg	laden: unladen: overloaded [1]:	$m_B = 35{,}250$ kg 6220 kg 39,250 kg
CG position	$b_A = 2.56$ m, $h_A = 1.13$ m	laden: unladen: laden f [2]: laden r [2]:	$b_B = 2.42$ m, $h_B = 2.23$ m 1.47 m 1.15 m 5 m 2.23 m 1.42 m 2.23 m
coupling position	$c_A = 0.43$ m, $h_{sA} = 0.85$ m		$c_B = 7.7$ m, $h_{sB} = 0.85$ m
wheels [3]	tyre: 395/70R19.5 $r_{dA} = 0.494$ m $I_{kA1} = 8$ kg·m², $I_{kA2} = 14$ kg·m²		tyre: 395/70R19.5 $r_{dB} = 0.494$ m $I_{kB2} = 8$ kg·m²
forces of resistance	$h_{pA} = 1.832$ m, $A_A = 9.014$ m², $c_{xA} = 0.8$, $\rho = 1.2$ kg/m³ $f = 0.01$, $A_t = 4.7 \times 10^{-4}$ s²/m²		$h_{pB} = 2$ m, $\Delta A_B = 0.732$ m², $c_{xB} = 1$, $\Delta c_x = 0.2$, $\rho = 1.2$ kg/m³ $f = 0.01$, $A_t = 4.7 \times 10^{-4}$ s²/m²

[1] overload only for case b4 (in which CG position is as nominal (laden), [2] laden f/r—concerns cases b3f/r, [3] A1, B2—single tyres, A2—twin tyres.

Table 2 presents the values of the coefficients of the tangential force model in the tyre-road contact. They were selected in such a way as to obtain the values of the friction coefficients as can be found, e.g., in [43,74,75] for the three considered road surface conditions: nominal (it corresponds to a dry asphalt surface) and with reduced adhesion (it corresponds to a wet asphalt surface and ice-covered surface). Figure 6 shows the corresponding unit characteristics of the tangential force.

Table 2. Modified Burckhardt tyre-road model parameters.

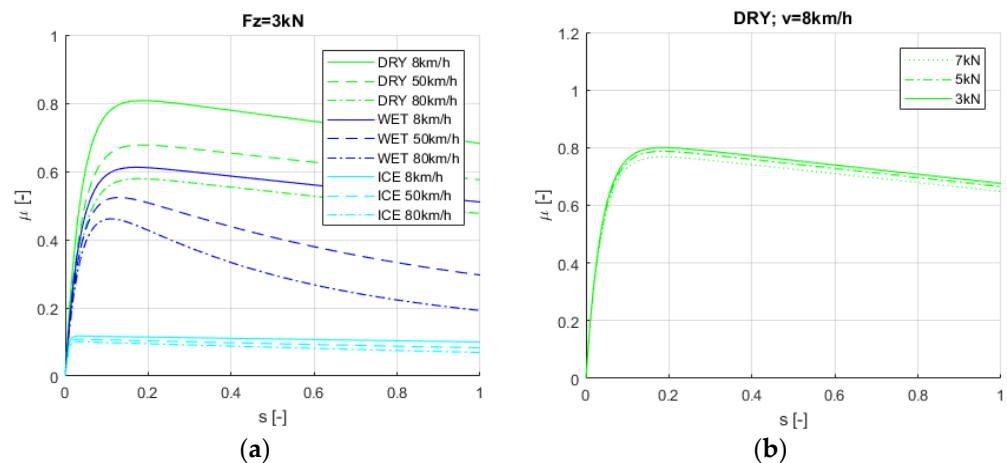|	c_1	c_2	c_3	c_5	c_{p1}	c_{p2}	c_{p3}	c_{p4}
Nominal **(dry)**	0.87	26.5	0.19	10^{-11}	-0.006	1.1	0.016	0.004
Reduced friction **(wet)**	0.65	28.5	0.21	10^{-11}	-0.003	1.8	0.09	0.004
Reduced friction **(ice)**	0.12	206	0.031	10^{-11}	-0.003	1.8	0.016	0.001

Figure 6. Tyre-road unit longitudinal force characteristics: (**a**) For different vehicle speed; (**b**) For different normal forces.

### 3.2. Braking System Parameters—Braking Force Distribution

Achieving a perfect distribution of braking forces between individual axles is practically impossible in real solutions. Therefore, for towing vehicles intended for the transport of goods and towed vehicles (excluding semitrailers), the regulation [29] specifies the permissible limits of deviation, the so-called utilized adhesion index f_i of individual axles (where f is the ratio of the braking force to the normal reaction of the ground) from the ideal distribution. In [29], each part of the vehicles set is treated as a single vehicle without considering the brake control of the towed vehicles. To ensure the compatibility of the braking forces in the set of vehicles, the permissible bands of changes, the so-called computational braking ratios of both vehicles γ_{hA} i γ_{hB} (expressing the ratio of generated vehicle braking forces to its weight). These bands are defined for the vehicles for their extreme load conditions (unloaded/unladen and fully loaded/laden) as a function of the control pressure p_m on the coupling head.

The parameters of the braking system model of the tested vehicles set were selected to reflect the actual operation of the pneumatic braking system as realistically as possible and to meet the requirements mentioned above for stability (brake force distribution) and compatibility of braking systems according to ECE [29]. Figure 7 shows the selected characteristics of the indexes of utilized adhesion f_{A1} and f_{A2} for the tractor axles against the permissible bands determined by the conditions [29]:

$$solution\ I: \begin{cases} f_{A1}, f_{A2} \le \frac{\gamma_{hA}+0.07}{0.85} \text{ for } \gamma_{hA} = 0.1 \div 0.61 \text{ (line AB)} \\ f_{A1} > \gamma_{hA} > f_{A2} \text{ for } \gamma_{hA} = 0.15 \div 0.30 \text{ (line CD)} \end{cases} \tag{27}$$

or

$$solution\ II: \begin{cases} f_{A1} \ge \gamma_{hA} - 0.08 \text{ for } \gamma_{hA} = 0.15 \div 0.3 \text{ (line MN)} \\ f_{A1}, f_{A2} \le \gamma_{hA} + 0.08 \text{ for } \gamma_{hA} = 0.15 \div 0.3 \text{ (line JK)} \\ f_{A2} \le \frac{\gamma_{hA}-0.3}{0.74} + 0.38 \text{ for } \gamma_{hA} \ge 0.3 \text{ (line KB)} \end{cases} \tag{28}$$
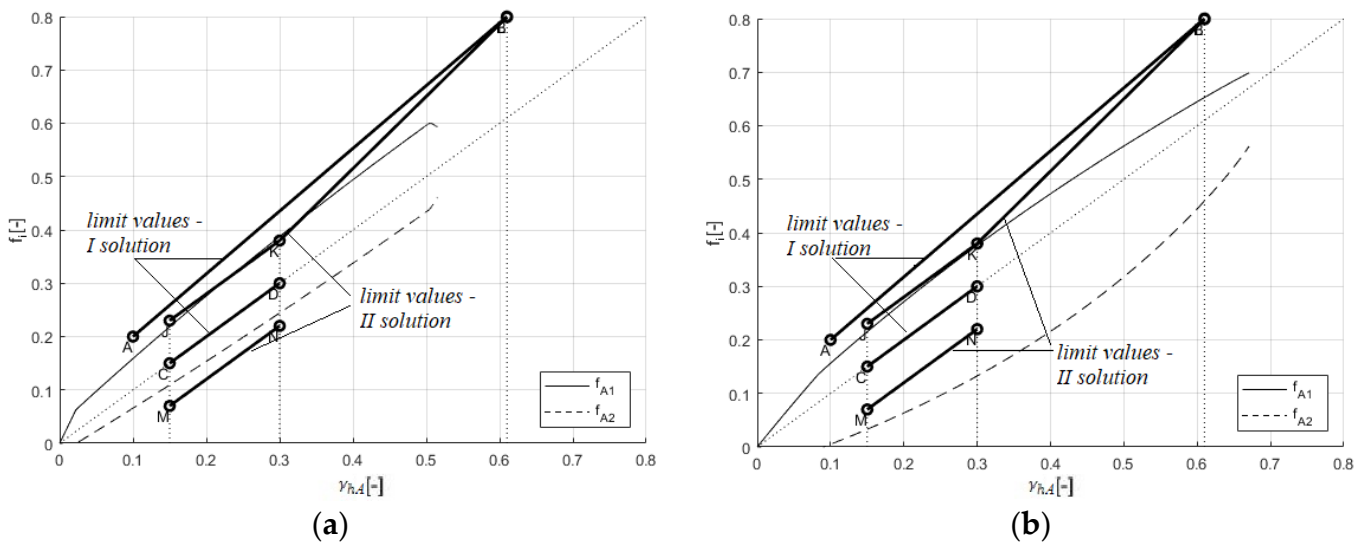
Figure 7. Characteristics of indexes of utilized adhesion of tractor axles f_{A1} and f_{A2} against the background of the requirements specified in [29]: (**a**) A tractor with an equivalent coupling load simulating a laden semitrailer; (**b**) A tractor with an equivalent coupling load simulating a unladen semitrailer.

Figure 8 furthermore shows the characteristics illustrating the computational braking ratio of the tractor (a) and the semitrailer (b) as a function of the pressure in the coupling head p_m. The required bands given in [29] are also plotted.

(a)

(b)
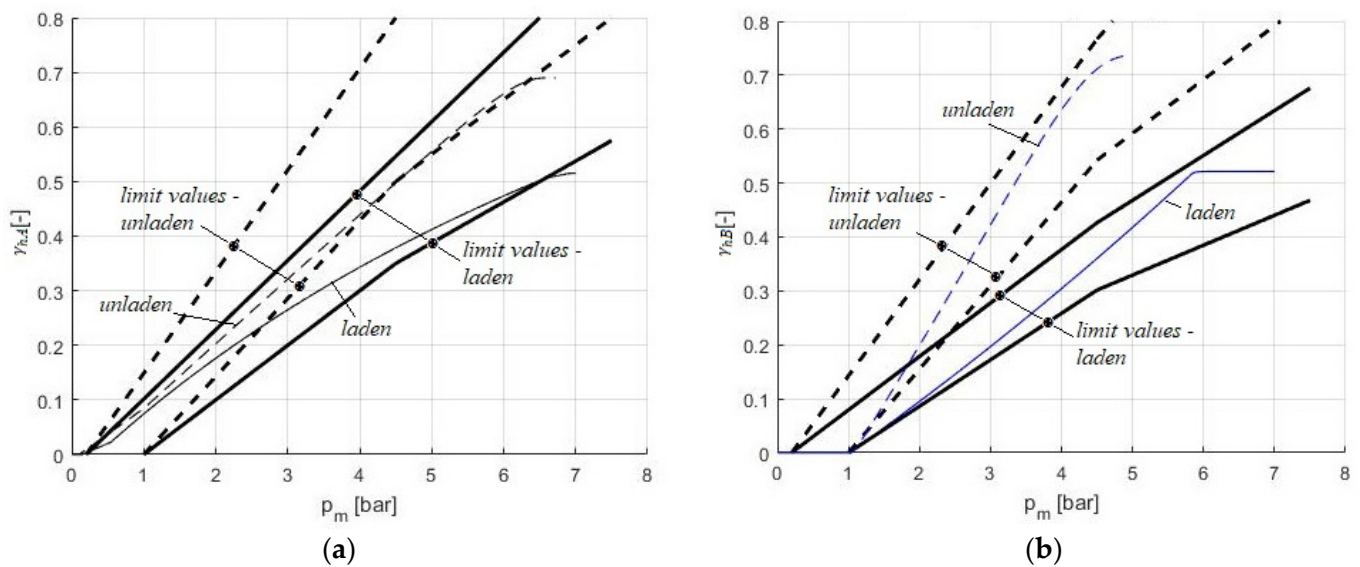
Figure 8. Characteristics of the computational braking ratio as a function of pressure in the coupling head: (**a**) A tractor with an equivalent coupling load simulating a laden and unladen semitrailer; (**b**) A laden and unladen semitrailer.

3.3. Adopted Conditions of the Braking Maneuver

The calculations assume that the braking process starts at the initial time t = 0 with the initial conditions:

$$v_s = 20 \text{ m/s (72 km/h)}, \omega_{ki} = 40.5 \text{ rad/s}$$

In the brake system model, the input is the position of the main control valve adjuster of the pneumatic actuation system. It was assumed, for comparison, to carry out two calculation cycles for the adopted variants b1 . . . 8, named:

- Constant excitation (α = const = 45°, the same position of the main control valve adjuster in variants b1 . . . 8)—hereinafter denoted as CE.
- Constant deceleration (α = var, the angle α in each variant b1...8 is selected to obtain approximately the same deceleration value in the phase of fully developed braking)—hereinafter denoted as CD.

The final effect of the braking system model is the time history of the given braking moments on vehicles' axles. Figure 9 presents such histories. They are examples but correspond to the real ones that can be found for the analyzed vehicles. The driver's reaction time is omitted, and the rise times are assumed at the level of the so-called emergency braking. The values of the maximum braking torques and the response times result from the catalogue data of the brake system components (for the maximum working pressure) [69,70,76] and the characteristics of the brake actuators and brake mechanisms ([67,68]). The response time of the pressures, as well as the response time of the braking system and the torque rise time for the individual axles of the set, are summarized in Table 3. Reaction times on the pneumatic lines were selected so that the total response times were comparable with the available research in the literature [15,30,77,78]. The course shown in Figure 9 was applied to the CE (constant excitation) calculation cycle.
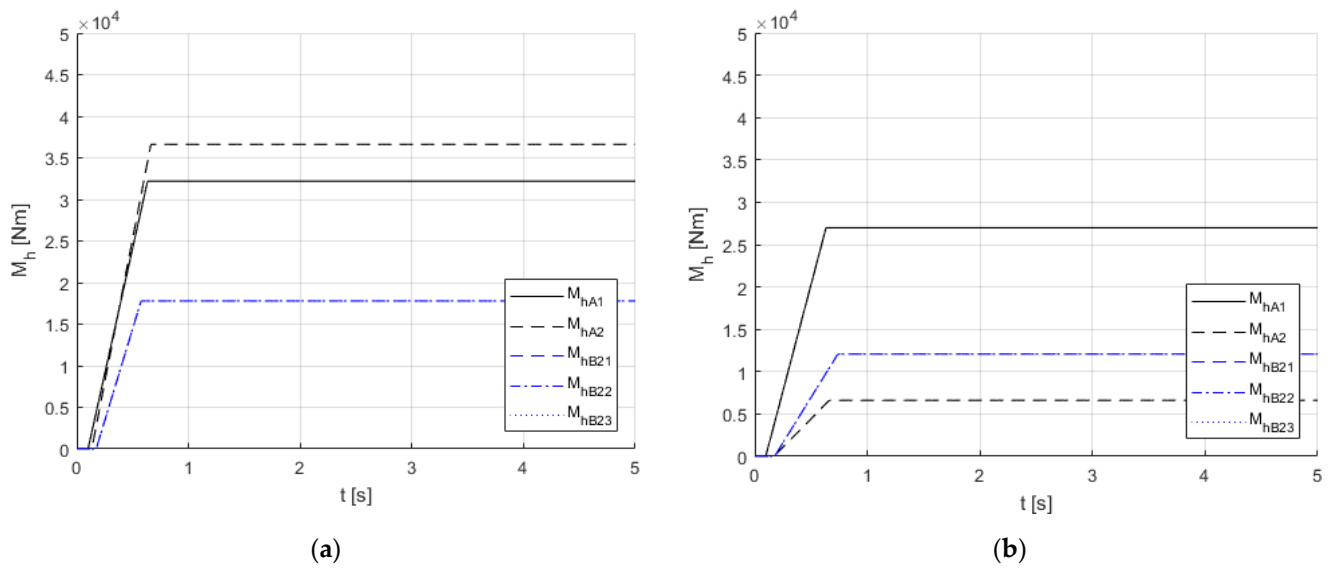
Figure 9. The course of excitation—given braking torques of the tractor axle and the semitrailer axle for the CE cycle—with the same position of the main control valve adjuster $\alpha = 45°$: (**a**) Semitraler laden; (**b**) Semitraler unladen.

Table 3. Response times of pressures and braking moments as well as rise times of braking moments on individual axes, in seconds.

Axle	Loaded Vehicle			Empty Vehicle		
	Response Time of Pressure	Moment	Rise Time of Moment	Response Time of Pressure	Moment	Rise Time of Moment
p_h	0.05	-	-	0.05	-	-
A1	0.075	0.1	0.63	0.06	0.1	0.63
A2	0.11	0.13	0.66	0.08	0.17	0.66
p_m	0.09	-	-	0.09	-	-
B2	0.155	0.17	0.58	0.155	0.17	0.74
B2 *	0.355	0.37	0.78	-	-	-

p_h—pressure downstream of the main control valve, p_m—pressure in coupling head, * failure of the semitrailer braking system (longer reaction time)—variant b6.

As standard, calculations were made with the ABS switched off. In cases where the wheels were locked, the simulation was repeated with the model of the ABS turned on. The following parameters were adopted in the ABS model: s_{max}= 0.3, s_{min}= 0.1, Δp_{ABS} = 20/10 bar (pressure reduction/increase phase), Δt_{ABS} = 0.5 s.

3.4. Adopted Assessment Criteria

Some criteria for the analysis were adopted to assess the safety risks, which directly speak about the braking effectiveness and indirectly about the risk of loss of stability, including jack-knifing. The quantities proving the effectiveness are the braking time, deceleration (acceleration with the opposite sign) in the period of fully developed braking force and the braking distance. The additional criteria may be the circumferential deceleration $-a_{ki}$ of the wheels (circumferential acceleration $a_{ki} = \dot{\omega}_{ki} \cdot r_{di}$ with the opposite sign) and their circumferential velocities v_{ki}, indicating a tendency to the locking or its occurrence. In the context of the risk of jack-knifing, the first quantity is the horizontal force in the coupling (fifth wheel) F_{sA}. The sign and value of this force are essential criteria for assessing the risk of breaking the set. A positive value of the force F_{sA} (denoting the situation of the semitrailer "pressing" on the tractor) is a significant indication of such a threat. Another quantity is the slip ratio s_i of a given axle. Its high (excessive) value (e.g., close to 1) may indicate a potential lack of control over the vehicle (e.g., locking the steering axle means a

loss of handling, locking the wheels of the rear axle or the axle of a semitrailer implies a risk of losing longitudinal and lateral stability). The order of locking the wheels of individual axles together with force in the coupling suggests the possibility of jack-knifing or trailer skidding.

3.5. Simulation Results and Their Discussion

Figures 10–12 show the results of the simulation of braking of the nominal set (b1) in the case of constant excitation (CE). There are presented time histories of vertical and horizontal forces, accelerations, velocities, wheels' angular velocities and their slip ratios. Figures 13 and 14 show selected results (horizontal forces and velocities) for other considered vehicle set variants. The histories presented in Figures 10–14 refer to cases in which the ABS was inactive. For comparison, Figure 15 shows, but only for the b7 variant, the results with the ABS turned on.
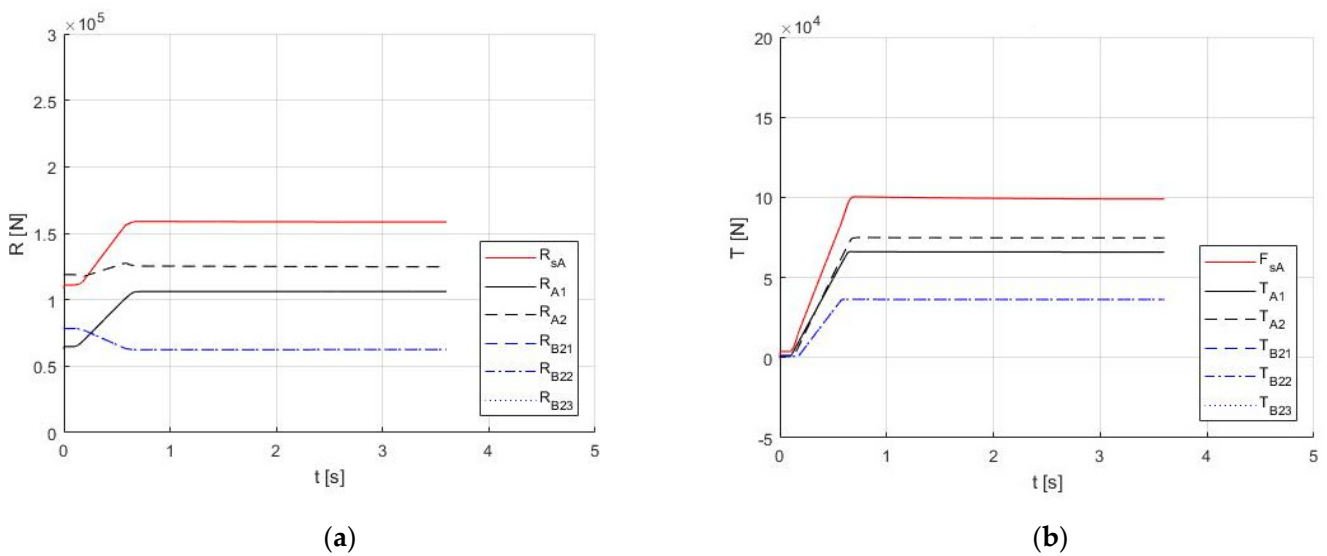
Figure 10. Time histories for variant b1, CE, ABS off: (**a**) Vertical forces; (**b**) Horizontal forces.
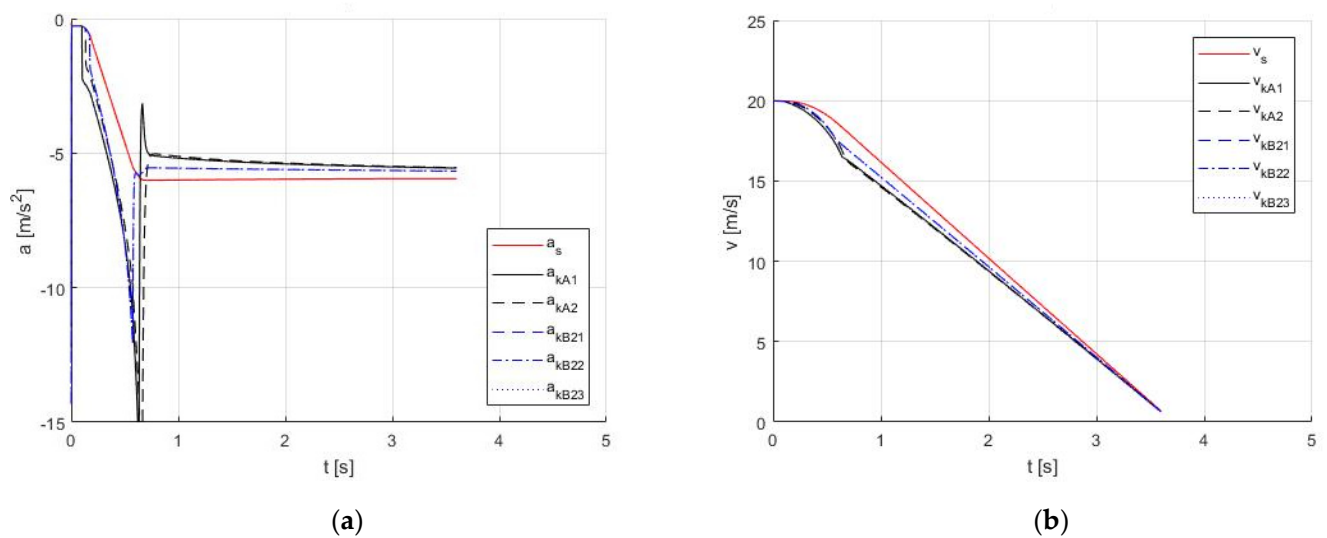
Figure 11. Time histories for variant b1, CE, ABS off: (**a**) Accelerations; (**b**) Velocities.
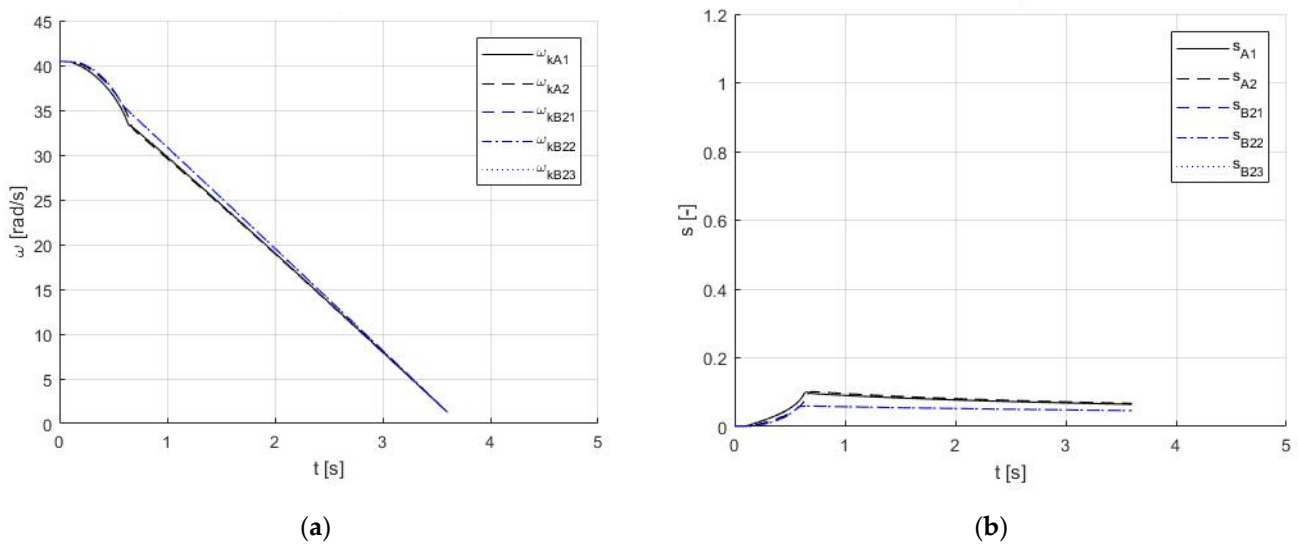
(**a**)
(**b**)

Figure 12. Time histories for variant b1, CE, ABS off: (**a**) Angular velocities; (**b**) Slip ratios.

In the case of b1 assumed as the nominal (reference case), the force in the coupling reaches approximately 100 kN and neither wheel locks (with ABS disengaged). It results from the adopted parameters of the braking system and the selection of the maximum position of the main control valve positioner for the adopted simulation conditions b1. Figure 11a reveals a potential wheel lockup tendency in the form of a high circumferential deceleration gradient of the wheels. The deceleration of the set (in the phase of full braking) was 6.0 m/s^2, and the braking distance was 40.0 m. The other cases were analysed similarly. Table 4 presents synthetically the effects of the analysis of all tests with constant excitation (CE) in the form of quantitative and qualitative indicators describing the braking process of the set of vehicles. In a similar way, Table 5 presents the effects of the analysis for the simulations with the same deceleration (CD). Since, in this case, the quantitative measures of braking efficiency were similar for individual set variants (braking time approx. 4.7 s and braking distance approx. 50 m), the table is limited to the presentation of horizontal force in the coupling and the effect of wheel locking.
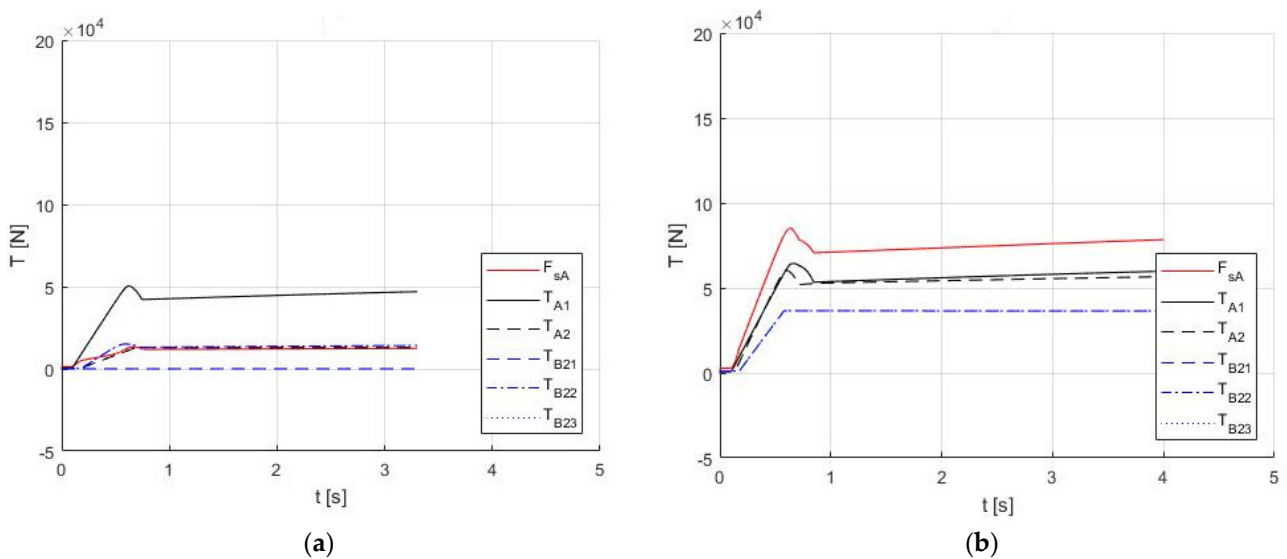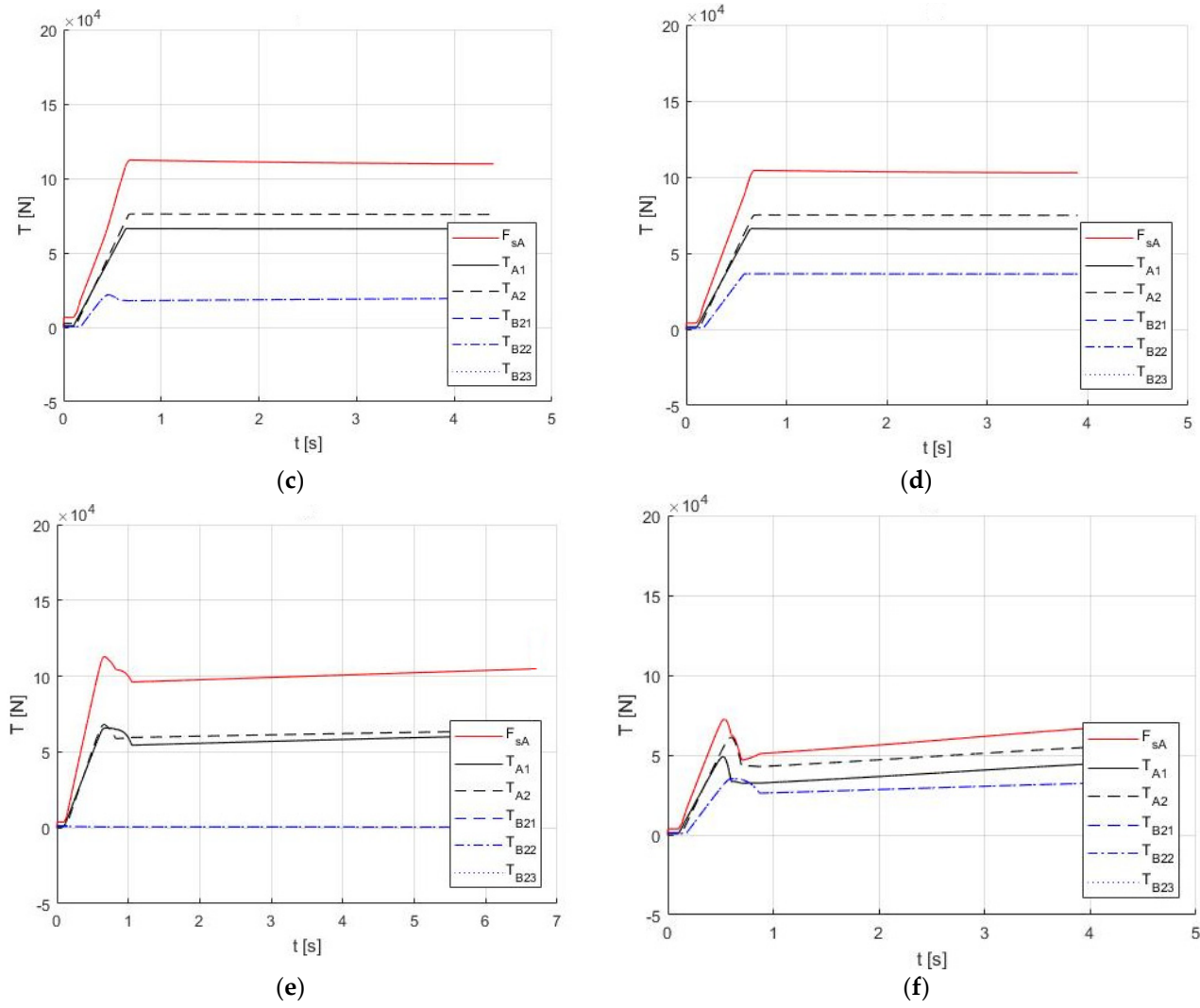

(**a**)
(**b**)

Figure 13. *Cont*.

Figure 13. Time histories of horizontal forces, CE, ABS off: (**a**) b2; (**b**) b3r; (**c**) b3f; (**d**) b4; (**e**) b5; (**f**) b7.
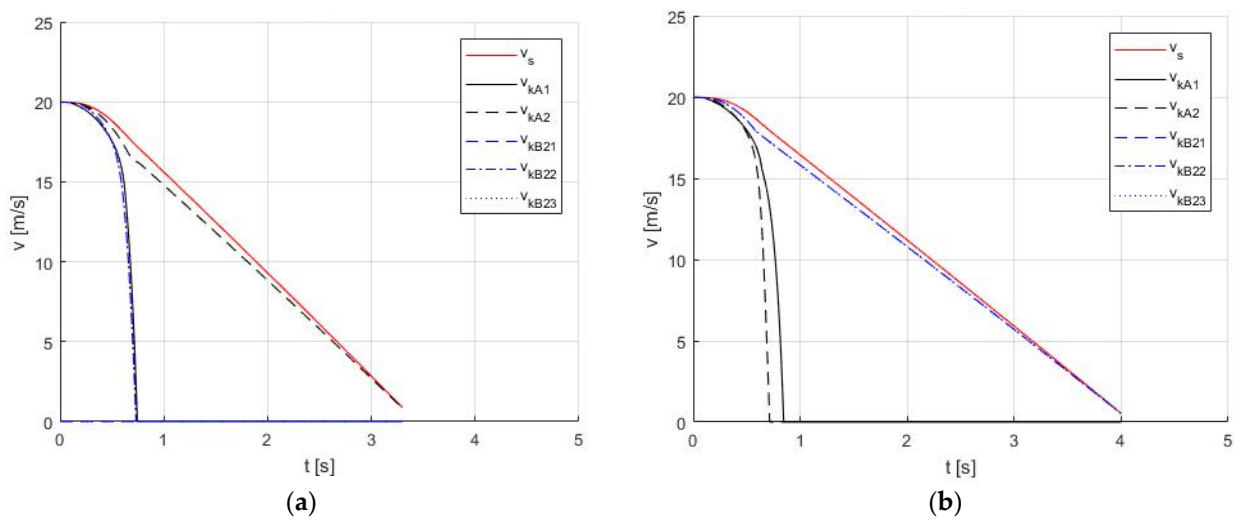
Figure 14. *Cont.*
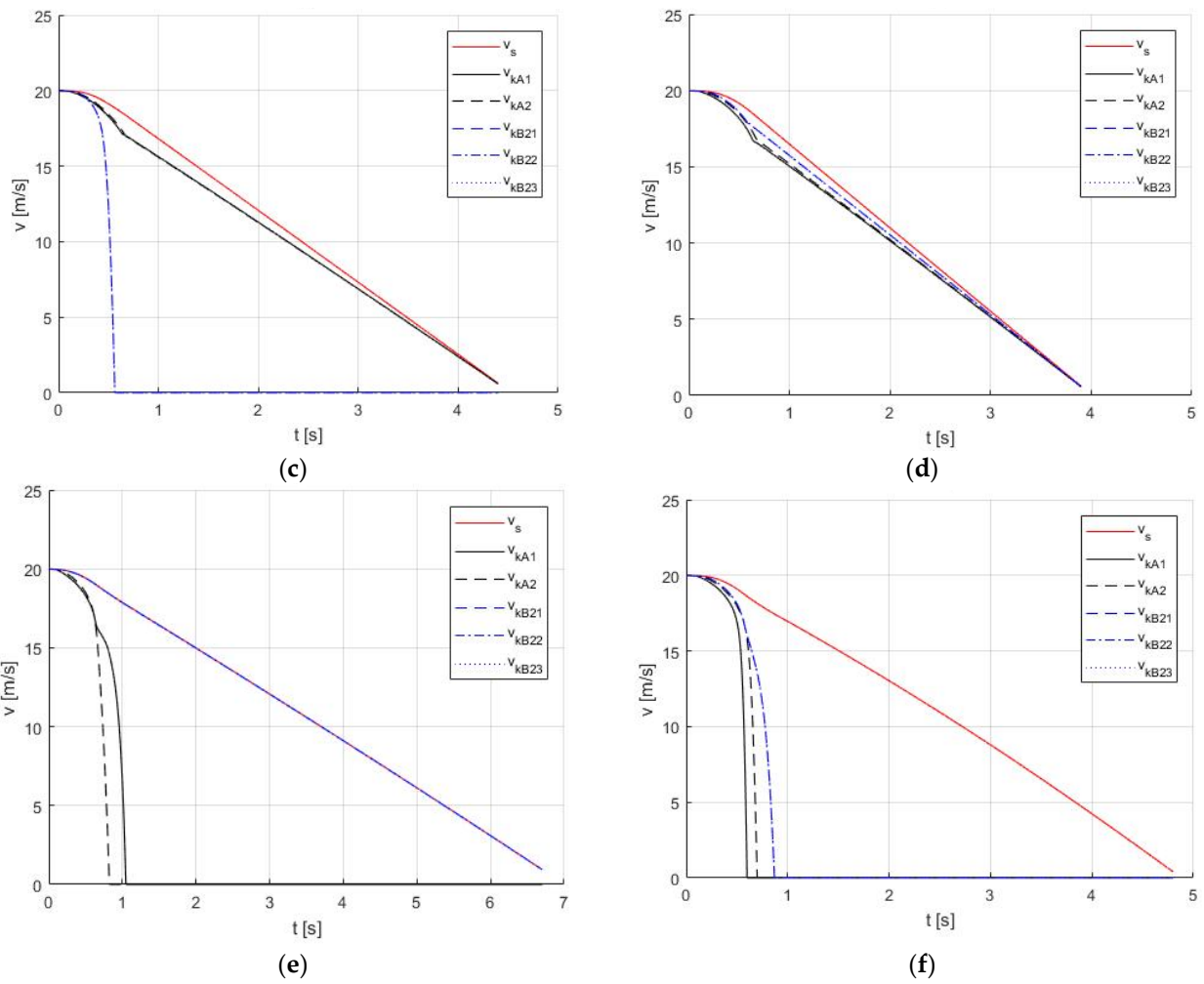
Figure 14. Time histories of velocities, CE, ABS off: (**a**) b2; (**b**) b3r; (**c**) b3f; (**d**) b4; (**e**) b5; (**f**) b7.
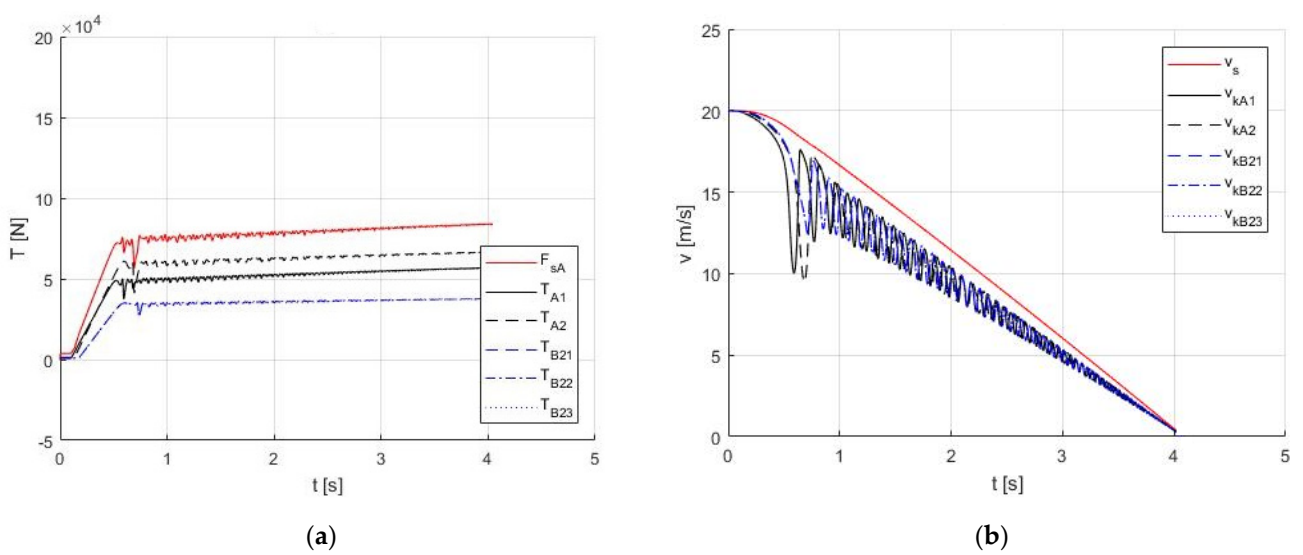

Figure 15. Time histories for variant b7, CE with ABS turned on: (**a**) Horizontal forces; (**b**) Velocities.

Table 4. Synthetic (qualitative) safety assessment of the braking process for constant excitation series (CE) for 9 braking variants (symbols ↑↓ mean a downward or upward trend in relation to the reference case—nominal b1). In parentheses, the values for the case of active ABS are given.

	b1	b2	b3r	b3f	b4	b5	b6	b7	b8
					Constant Excitation ($\alpha = 45°$)				
					Coupling force F_{sA}				
IB	>0	>0	>0	>0	>0	>0	>0	>0	>0
	0 ÷ 100 kN	0 ÷ 14 kN ↓ (0 ÷ 17 kN ↓)	0 ÷ 85 kN ↓ (0 ÷ 89 kN ↓)	0 ÷ 112 kN ↑ (0 ÷ 111 kN ↑)	0 ÷ 104 kN ↑	0 ÷ 113 kN ↑ (0 ÷ 113 kN ↑)	0 ÷ 105 kN ↑	0 ÷ 72 kN ↓ (0 ÷ 76 kN ↓)	0 ÷ 12 kN ↓ (0 ÷ 14 kN ↓)
FD	>0	>0	>0	>0	>0	>0	>0	>0	>0
	100 kN	12 kN ↓ (14 kN ↓)	71 ÷ 77 kN ↓ (~89 kN ↓)	112 kN ↑ (108 ÷ 111kN ↑)	104 kN ↑	98 ÷ 103 kN ↑ (113 ÷ 117kN ↑)	100 kN	50 ÷ 70 kN ↓ (76 ÷ 84 kN ↓)	12 kN ↓ (11 ÷ 14 kN ↓)
					Wheels locking				
A1	lack	YES (lack)	YES (lack)	lack	lack	YES (lack)	lack	YES (lack)	YES (lack)
A2	lack	lack	YES (lack)	lack	lack	YES (lack)	lack	YES (lack)	YES (lack)
B2	lack	YES (lack)	brak	YES (lack)	lack	lack	lack	YES (lack)	YES (lack)
					Tendency to wheels locking				
A1	YES	n/a (YES)	n/a (YES)	YES	YES	n/a (YES)	YES	n/a (YES)	n/a (YES)
A2	YES	YES	n/a (YES)	YES	YES	n/a (YES)	YES	n/a (YES)	n/a (YES)
B2	YES	n/a (YES)	YES	n/a (YES)	YES	lack	YES	n/a (YES)	n/a (YES)
					Order of locking the axes				
	n/a	proper	bad	bad	n/a	bad	n/a	proper	proper
					Deceleration FD				
	6.0 m/s²	6.3 ÷ 6.6 m/s² ↑ (7.0 ÷ 7.5 m/s² ↑)	5.3 m/s² ↓ (5.7 m/s² ↓)	4.7 m/s² ↓ (4.9 m/s² ↓)	5.5 m/s² ↓	3.0 m/s² ↓ (3.4 m/s² ↓)	6.0 m/s²	3.7 ÷ 4.8 m/s² ↓ (5.0 ÷ 5.6 m/s² ↓)	1.0 m/s² ↓ (1.0 ÷ 1.1 m/s² ↓)
					Mean deceleration IB+FD				
	5.7 m/s²	5.8 m/s² ↑ (6.5 m/s² ↑)	4.9 m/s² ↓ (5.2 m/s² ↓)	4.3 m/s² ↓ (4.6 m/s² ↓)	5.0 m/s² ↓	2.8 m/s² ↓ (3.2 m/s² ↓)	5.3 m/s² ↓	4.1 m/s² ↓ (4.9 m/s² ↓)	1.0 m/s² ↓ (1.0 m/s² ↓)
					Braking time				
	3.7 s	3.3 s ↓ (3.1 s ↓)	4.0 s ↑ (3.8 s ↑)	4.5 s ↑ (4.3 s ↑)	4.0 s ↑	7.0 s ↑ (6.2 s ↑)	3.8 s ↑	4.8 s ↑ (4.0 s ↑)	21 s ↑ (19 s ↑)
					Braking distance				
	40 m	37 m ↓ (34 m ↓)	44 m ↑ (42 m ↑)	48 m ↑ (47 m ↑)	43 m ↑	73 m ↑ (66 m ↑)	42 m ↑	53 m ↑ (44 m ↑)	207 m ↑ (191 m ↑)

IB—brake initialization phase, FD—fully developed braking phase.

Table 5. Synthetic (qualitative) safety assessment of the braking process for constant deceleration series (CD) for 9 braking variants (symbols ↑↓ mean a downward or upward trend in relation to the reference case—nominal b1). In parentheses, the values for the case of active ABS are given.

	b1	b2	b3r	b3f	b4	b5 *	b6	b7	b8 *
				Constant Deceleration (a $\cong$ −4.5 m/s²)					
					Excitation α				
	26°	20°	26°	35° (34°)	28°	-	26°	26°	-
					Coupling force F_{sA}				
IB	>0	>0	>0	>0	>0	-	>0	>0	-
	0 ÷ 62 kN	0 ÷ 7 kN ↓	0 ÷ 61 kN ↓	0 ÷ 101 kN ↑ (96 kN ↑)	0 ÷ 71 kN ↑	-	0 ÷ 71 kN ↑	0 ÷ 62 kN	-
FD	>0	>0	>0	>0	>0	-	>0	>0	-
	58 kN	2.5 kN ↓	57 kN ↓	99 kN ↑ (95 kN ↑)	~67 kN ↑	-	58 kN	58 kN	-
					Wheels locking				
	lack	lack	lack	as in Table 4	lack	-	lack	lack	-

IB—brake initialization phase, FD—fully developed braking phase, * it is not possible to achieve the target deceleration.

A graphical interpretation of the above tables in terms of selected parameters of tractor-semitrailer set on the braking safety indicators is shown in Figures 16–18.

The results in Tables 4 and 5 show that in all tests of the braking of the tractor-trailer combination—variants b1 to b8 for the case of the same position of the main control valve adjuster (CE) and the individual position of this adjuster at which the deceleration in the fully developed braking phase was c.a. 4.5 m/s² (CD), the horizontal force in the coupling is positive. The obvious result is that the combination with an unladen semitrailer (b2) shows the lowest value of the horizontal force in the coupling (up to a maximum of 17 kN). The horizontal force in the coupling is greatly influenced by the shift of the centre of gravity (b3r and b3f). The simulation with a rearward shift of the centre of gravity (b3r) shows a lower than the nominal (b1) value of the F_{sA} force (its value is at the level of 71 ÷ 77 kN in

the phase of fully developed braking in b3r variant, where for b1 case is c.a 100 kN). This means that loading of the semi-trailer axle (as in b3r variant), resulting in an increase in the adhesion utilization rate, has a positive effect on reducing the risk of braking safety. From the other hand, in the simulation with the centre of gravity shifted forward (b3f), the horizontal force in the coupling is $8 \div 12$ kN higher than the nominal variant (b1) value. The braking results with a constant deceleration of 4.5 m/s^2 (CD) are similar in terms of quality.
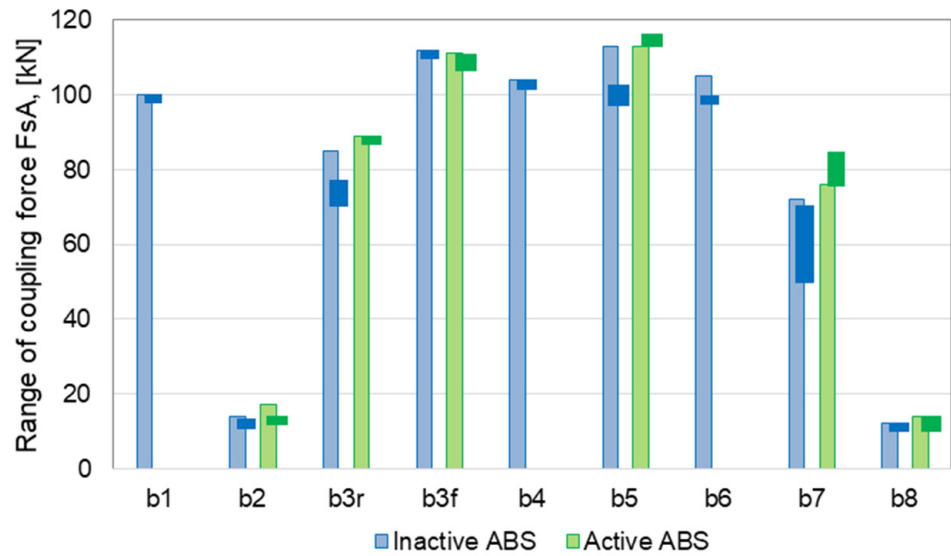

Figure 16. Range of coupling force for constant excitation series (CE) for 9 braking variants (lighter colour—braking initialization phase IB, darker colour—fully developed braking phase FD).
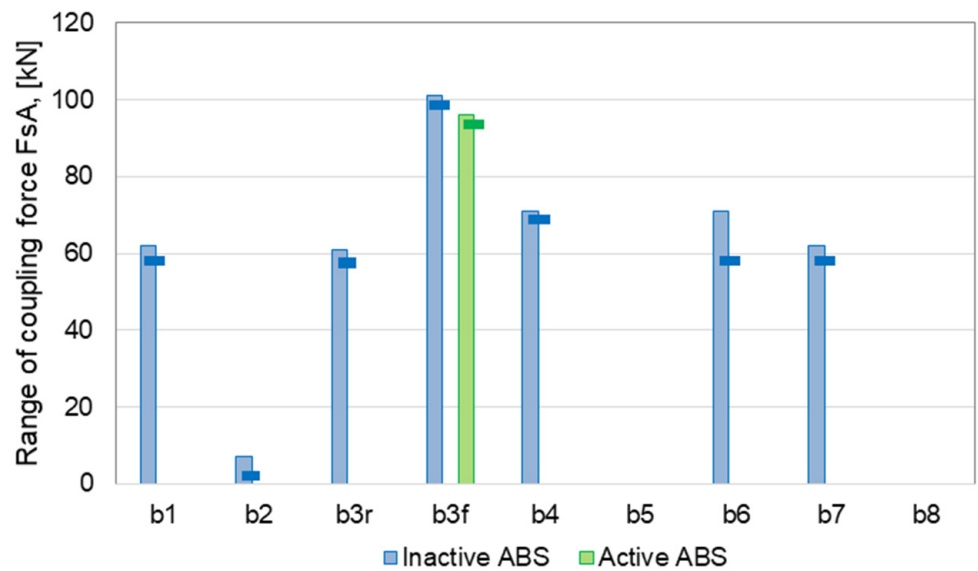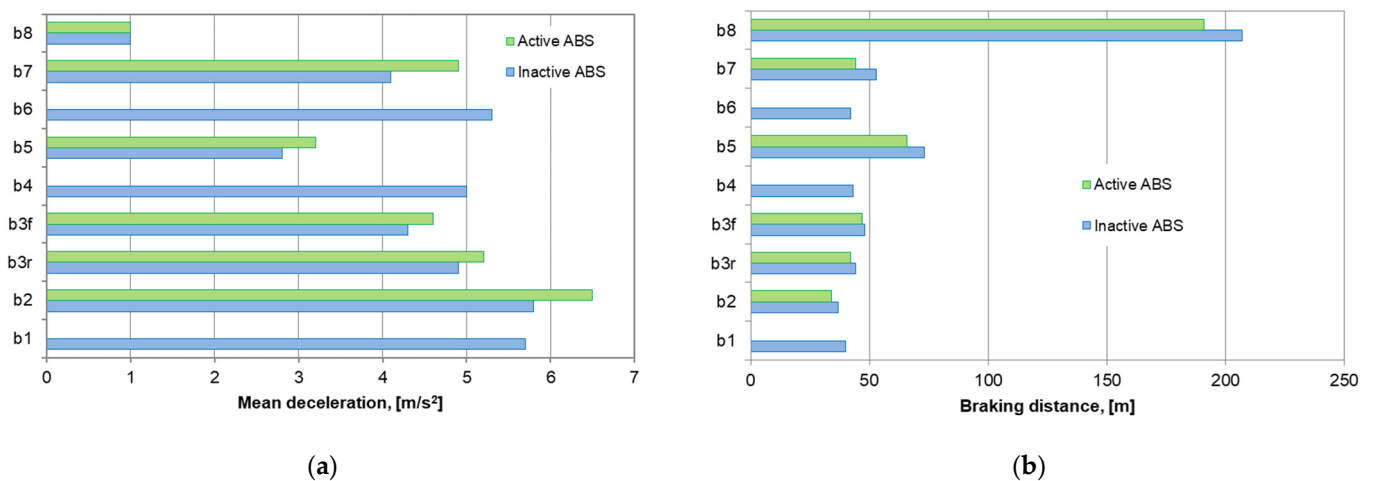

Figure 17. Range of coupling force for constant deceleration series (CD) for 9 braking variants (lighter colour—braking initialization phase IB, darker colour—fully developed braking phase FD).

(**a**)

(**b**)

Figure 18. Mean deceleration and braking distance force for constant excitation series (CE) for 9 braking variants: (**a**) Mean deceleration; (**b**) Braking distance.

The highest value of the horizontal force in the coupling was obtained for the simulation with an unbraked semi-trailer (b5), in which the coupling force is a maximum of 113 kN for ABS off and 117 kN for ABS on. ABS, the maximum force in the coupling is similar to the case of b3f. However, in b5, in the phase of fully developed braking, it is even approx. 12 kN lower than in b3f. From this, it follows that case b3f (centre of gravity shifted forward) is even worse than no trailer braking (b5).

In the variant with longer reaction time (b6), an increase in the maximum value of the horizontal force in the coupling in the phase of applying the brakes (IB) is noticeable. However, the increase in these forces is not significantly large (by 5 kN in the CE simulation and 9 kN in the CD simulation). From the other hand, in the phase of fully developed braking (FD), the force F_{sA} in the coupling is identical to this in the nominal variant (the maximum braking torque for the axle of the semi-trailer is reached). A greater value of the maximum force in the coupling in the brake initialization phase (IB) than in the fully developed braking phase (FD) in the nominal variant b1 (CE) did not occur, and this effect becomes visible with the increase in the response time of the semi-trailer braking system. In the moment when F_{sA} reach maximum the risk of jack-knifing phenomena is greatest. This topic will also be discussed later in this section.

Also, higher than the value of the F_{sA} force in the nominal variant is shown by the variant with exceeded load mass b4 (by 4 kN for the CD case and by 9 kN for the CE case). In b7 variant (braking on a surface with reduced adhesion—wet surface) for the CE case the horizontal force in the coupling is lower than the nominal variant (b1) value. This may be due to the fact that get less deceleration (see Table 4 and Figure 18). This is also justified by the tests with the same deceleration (CD), where the horizontal forces in the coupling are approximately similar for both variants b1 and b7.

Comparing the results when braking on a road with very low adhesion (b8), the obtained results are qualitatively in line with the expected ones. The braking performance indicators have obviously deteriorated. The operation of the anti-lock braking system improves efficiency. An important effect is the reduction of the horizontal coupling force. However, it should be remembered that due to the lower ability to transfer forces in wheel-road contact also in the vertical direction, it is difficult to conclude on this basis about a lower risk of e.g., of jack-knifing phenomena. It follows from this that the type of surface does not directly affect the horizontal force in the coupling, but it does affect the maximum deceleration obtained. Thus, this is a different effect than, for example, in variants b3f or b4, where the increase in the horizontal force in the coupling was directly caused by the change in mass and the position of the centre of gravity. This can be seen by comparing the results for tests with the same deceleration (CD simulations)—see Table 5 and Figure 17.

A recurring feature in most of the presented simulations, both for the maximum position of the main control valve positioner (CE) and for the same deceleration in the phase of fully developed braking (CD), is the moment when the horizontal force in the coupling reaches the highest value. It occurs in the final phase of actuating the brakes before the phase of fully developed and stabilized braking. This is related to the reaction time of individual axles of the braking system or the order of axle blocking resulting from the load on axles. The braking process in the phase of actuating the brakes is unstable, and large changes of tangential forces and the angular decelerations of the wheels occur then (e.g., Figure 11a). This is the moment when the risk of braking safety is most significant.

The wheel locking order and the status of ABS activation affect the horizontal force in the coupling. Blocking the wheels of vehicle A first (e.g., variant b3r) reduces the braking ratio of this vehicle and thus reduces the force in the coupling. In the b3r variant, the horizontal force in the coupling decreased (compared to the nominal variant), and it increased in the opposite case—b3f. Also, the activity of the ABS significantly affects the values of the horizontal forces in the coupling. In mentioned the case of b3r, after switching on the ABS, the force in the coupling in the phase of fully developed braking increased from 71 ÷ 77 kN to about 89 kN. A similar effect can be seen in the b7 variant, where the higher (by approx. 20 kN) value of the force in the coupling was observed for braking with the ABS on in the phase of fully developed braking. From the other hand, in the case of b3f, active ABS reduced slightly the horizontal force in the coupling to 108 kN–111 kN. It is worth emphasizing, however, that this value is still higher than the nominal 100 kN. In general, ABS reduces the risk associated with braking safety, but does not eliminate it completely, and in some cases, as described above, even increases it.

For tests with constant excitation (CE), an incorrect axle locking order occurs for the simulation in the conditions of incorrectly distributed load (b3r, b3f) and failure of the braking system (b5). In the b3r and b5 variants, the tractor's rear axle wheels are locked first—there is a risk of jack-knifing. In the case of b3f, the axle of the semitrailer is blocked—the risk of instability of the semitrailer. The variant b2 is a debatable issue, where the front axle of the tractor and the complex axle of the semitrailer are locked approximately simultaneously, while the rear axle of the tractor is not locked. In the case of tests with constant deceleration (CD), only in one variant (b3f), the wheels were locked with the ABS turned off, qualitatively the same as for the maximum excitation (CE).

Analysing the test results for the constant excitation (CE), it can be seen that each deviation from the nominal variant affects the braking efficiency measures. The set with a laden semitrailer (nominal b1) reached a deceleration of about 6.0 m/s^2, and the braking distance was up to 40 m. The shortest braking distance (37 m with ABS off and 34 m with ABS on) and the biggest average deceleration (5.8 ÷ 6.5 m/s^2) were obtained for the unladen semitrailer (b2). Longer braking distances are in the simulations for a shift of the centre of gravity forward b3f (centre of gravity shifted to the front of the semitrailer) and b3r (centre of gravity shifted to the rear of the semitrailer). For variant b3r the average deceleration is 4.9 m/s^2 (ABS off) and 5.2 m/s^2 (ABS on), and the braking distance is 42 ÷ 44 m. In the case of b3f average deceleration is 4.3 m/s^2 (ABS off) and 4.6 m/s^2 (ABS on), and the braking distance is 47 ÷ 48 m. In the latter case, it is worth recalling that we also have another unfavorable effect—an increased horizontal force in the coupling in relation to the nominal variant b1.

The longest braking distance (73 m for ABS off and 66 m for ABS on) on a dry surface was obtained for the variant with failure of the semitrailer braking system (b5). The extended time to reach the maximum braking torque of the semi-trailer in the case of b6 also reduced the average deceleration, which resulted in an extension of the braking distance by 2 m.

On a wet surface (b7), the braking distance is 53 m with the ABS off and 44 m with the ABS on (and the average deceleration is 4.1 m/s^2 and 4.9 m/s^2, respectively). On ice (b8) the braking distance is 207 m with the ABS off and 191 m with the ABS on (and the average deceleration in both ABS status cases is close to 1.0 m/s^2—slightly less than

1.0 m/s^2 with the ABS off and slightly greater than 1.0 m/s^2 with the ABS on). The ABS system's significant impact on these braking performance measures is evident here.

The presented results were compared in the scope of the main indicators of braking efficiency available in the literature (average deceleration, braking distance) obtained in actual road tests. A truck with a similar mass to the b2 variant shows decelerations in fully developed braking at the level of 6.27–7.67 m/s^2 [14]. The braking distance of the tractor with a partially loaded semitrailer with a set weight of approx. 22 t (i.e., approx. 9 t more than in the variant of b2) in [15] was given at approx. 41m, and its deceleration at approx. 5.7 ÷ 6.0 m/s^2. For the unloaded set (about 15 t), the braking distance was 30–32 m, and the deceleration was about 7.25 ÷ 7.5 m/s^2. In [16], the average deceleration for a loaded vehicle of similar mass to the variant b1 is 4.4 to 5.4 m/s^2. For a tractor with damaged trailer brakes (a variant close to b5), the deceleration was from 3.43 to 4.22 m/s^2 [16]. In addition to deceleration and braking distance, the horizontal force in the coupling was compared. In the work [79] you can find information on the value of this force for vehicles with parameters similar to cases b1 and b5 with small decelerations of 0.5–0.6 m/s^2 at the level of approx. 11 and 14 kN, respectively. In the simulation under similar conditions, values of approx. 12–15 and 13–16 kN were obtained. In sum, it can be assumed that the simulation tests' results are similar to the real ones. Slight differences compared to [15,16] may result from a different construction of sets for the US market (these are the results for a 3-axle truck and a 2-axle semitrailer) and, consequently, other load distribution and utilized adhesion indexes of individual axles for similar states loading.

4. Conclusions

The article presents an outline of the methodology that allows the analysis of the braking safety of a set of vehicles (articulated vehicle) in the form of a relatively simple mathematical model. The presented simulation calculations for selected braking cases of vehicles sets in the form of a tractor-semitrailer, reflecting realistic conditions (vehicle parameters, operational situations in traffic), indicate the possibility of such an assessment. It is possible to evaluate the basic indicators of braking efficiency (braking distance, braking intensity, braking time) as well as features indicating the risk of loss of motion stability (force in the coupling, state of rotation of the wheels of the set's vehicles). A preliminary comparison of the simulation results with the available results of experimental tests (taken from [14–16]) indicates a good agreement in terms of the main indicators of braking efficiency.

The greatest threat, both related to the braking efficiency and the increase in the force in the coupling, is associated with the lack of braking of the semitrailer axles or a significant reduction in its load. The weight and location of the centre of gravity of the load have a large impact on braking safety. The positioning of the load can significantly increase or decrease the force in the coupling. The order in which the axles are locked is also important. The braking reaction time of the semitrailer affects the maximum value of the horizontal force in the coupling during the braking initialization phase. However, in the phase of fully developed braking, it is no longer relevant to this force. Another thing is the moment when the maximum value of the horizontal force occurs (so the moment when the risk of jack-knifing the tractor-semitrailer is the highest). It usually takes place in the final phase of actuating the brakes before the phase of fully developed braking.

The condition of the pavement has no direct effect on the horizontal force in the coupling. However, it determines the maximum deceleration value, which affects the indicators of braking efficiency and thus changes the values of the coupling forces. ABS reduces the risk associated with braking safety in this context, but does not completely eliminate it.

The presented simulations were only an example of the capabilities of the model and the program written in the Matlab environment. An essential feature of the proposed method and model is its versatility—you can easily change the configuration of the vehicles set—the towing vehicle (truck/tractor) and towed (trailer/semitrailer), number and type

of vehicle axles. It is also important to reproduce the actual characteristics of the pneumatic braking system and the ability to set various operating conditions as well as obtain relatively quick results on potential threats during braking. However, one should also remember about certain limitations related to the above-mentioned simplicity of the model (rectilinear motion is considered, relative movements of unsprung masses, interactions resulting from road surface inhomogeneity, etc. are omitted).In the course of future works, further development of the method and its testing on other set configurations and operating conditions are planned.

References

1. A Small Statistical Yearbook of Poland 2022. GUS, Warsaw; 2022. Available online: https://stat.gov.pl/obszary-tematyczne/roczniki-statystyczne/roczniki-statystyczne/maly-rocznik-statystyczny-polski-2022,1,24.html (accessed on 6 October 2022). (In Polish)
2. European Commsion. Mobility and Transport—Statistical Pocketbook 2021. 2021. Available online: https://op.europa.eu/en/publication-detail/-/publication/14d7e768-1b50-11ec-b4fe-01aa75ed71a1 (accessed on 6 October 2022).
3. European Road Safety Observatory. Annual Statistical Report on Road Safety in the EU 2021. 2021. Available online: https://road-safety.transport.ec.europa.eu/statistics-and-analysis/data-and-analysis/annual-statistical-report_en (accessed on 6 October 2022).
4. European Commsion. Mobility and Transport- Road Safety Facts & Figures. Available online: https://ec.europa.eu/transport/road_safety/road-safety-facts-figures-1_en (accessed on 6 October 2022).
5. Road Accidents in Poland in 2021. Report of the Police Headquarters and Similar Reports from Previous Years. Available online: https://statystyka.policja.pl/st/ruch-drogowy/76562,Wypadki-drogowe-raporty-roczne.html (accessed on 6 October 2022). (In Polish)
6. Global Status Report on Road Safety 2018. Available online: https://www.who.int/publications/i/item/WHO-NMH-NVI-18.20 (accessed on 11 October 2022).
7. Studies of the National Road Safety Council. Available online: https://www.krbrd.gov.pl/pl/72-badania.html (accessed on 6 October 2022). (In Polish)
8. Kupiec, A.; Kupiec, J.; Jęsiek, Ł. Analysis of the causes of failures in trucks. *Autobusy Tech. Eksploat. Syst. Transp.* **2018**, *19*, 115–120. [CrossRef]
9. WHO. Road Traffic Injures. Available online: https://www.who.int/health-topics/road-safety#tab=tab_1 (accessed on 6 October 2022).
10. Wicher, J. *Motor Vehicles. The Safety of Motor Vehicles and Road Traffic*; WKiŁ: Sulejówek, Poland, 2012. (In Polish)
11. NHTSA. Vehicle Aggressivity and Fleet Compatibility Research. Available online: https://www.nhtsa.gov/crashworthiness/vehicle-aggressivity-and-fleet-compatibility-research (accessed on 10 November 2022).
12. Huanga, H.; Siddiquib, C.; Abdel-Atyc, M. Indexing crash worthiness and crash aggressivity by vehicle type. *Accid. Anal. Prev.* **2011**, *43*, 1364–1370. [CrossRef] [PubMed]
13. Backaitis, S.H. *Vehicle Compatibility in Automotive Crashes*; Society of Automotive Engineers: Warrendale, PA, USA, 2005.
14. Czech, P.; Kula, P.; Juzek, M.; Turoń, K.; Jędrusik, D. Braking process a heavy goods vehicle used for military purposes. *Autobusy* **2016**, *17*, 100–106. (In Polish)
15. Garrott, R.; Heitz, M.; Bean, B. *Experimental Measurement of the Stopping Performance of a Tractor-Semitrailer from Multiple Speeds*; DOT HS 811 488; U.S. Department of Transportation, National Highway Traffic Safety Administration: Washington, DC, USA, 2011.
16. Lascurain, M.B.; Capps, G.; Franzese, O. *Heavy and Overweight Vehicle Brake Testing: Combination Five-Axle Tractor-Flatbed Final Report*; U.S. Department of Transportation Federal Motor Carrier Safety Administration: Indianapolis, IN, USA, 2017. [CrossRef]

17.	Luty, W. Simulation-based analysis of the impact of vehicle mass on stopping distance. *Eksploat. I Niezawodn.-Maint. Reliab.* **2018**, *20*, 182–189. [CrossRef]

18.	Ondrus, J.; Vrabel, J.; Kolla, E. The influence of the vehicle weight on the selected vehicle braking characteristics. In Proceedings of the 22nd International Scientific on Conference Transport Means, Trasails, Lithuania, 3–5 October 2018; pp. 384–390.

19.	Skrucany, T.; Vrabel, J.; Kazimir, P. The influence of the cargo weight and its position on the braking characteristics of light commercial vehicles. *Open Eng.* **2020**, *10*, 154–165. [CrossRef]

20.	Vrabel, J.; Jagelcak, J.; Zamecnik, J.; Caban, J. Influence of Emergency Braking on Changes of the Axle Load of Vehicles Transporting Solid Bulk Substrates. *Transp. Sci. Technol.* **2017**, *187*, 89–99. [CrossRef]

21.	Janczur, R.; Zawałeń, J. Braking parameters of trucks and buses in the reconstruction and analysis of road accidents. *Paragraf Na Drodze* **2021**, *2021*, 105–120. (In Polish)

22.	Ren, H.; Zhecheng, J. Study on braking stability of commercial vehicles: An optimized air brake system. *Adv. Mech. Eng.* **2019**, *11*, 1687814019848593. [CrossRef]

23.	Marienka, P.; Frančák, M.; Jagelčák, J.; Synáka, F. Comparison of Braking Characteristics of Solo Vehicle and Selected Types of Vehicle Combinations. *Transp. Res. Procedia* **2020**, *44*, 40–46. [CrossRef]

24.	Świder, P.; Bułka, D. Braking a car with a trailer without brakes. In Proceedings of the International Science-Technical Conference, Kielce-Ameliówka, Poland, 22–24 February 2016; pp. 376–382.

25.	Kamiński, Z. *Simulation and Experimental Testing of the Pneumatic Brake Systems of Agricultural Vehicles*; Publishing House of the Białystok University of Technology: Białystok, Poland, 2012.

26.	Jacobson, B. *Vehicle Dynamics Compendium for Course MMF062*; Chalmers University of Technology: Gothenburg, Sweden, 2016.

27.	Mitschke, M.; Wallentowitz, H. *Dynamik Der Kraftfahrzeuge*; Springer Nature: Berlin/Heidelberg, Gremany, 2014. [CrossRef]

28.	Prochowski, L. *Car Vehicles. Movement Mechanics*; WKŁ: Sulejówek, Poland, 2016. (In Polish)

29.	Regulation No 13 of the Economic Commission for Europe of the United Nations (UN/ECE)—Uniform Provisions Concerning the Approval of Vehicles of Categories M, N and O with Regard to Braking [2016/194] (OJ L 42 18.02.2016, p. 1, ELI), Belgium. 2016. Available online: http://data.europa.eu/eli/reg/2016/194/oj) (accessed on 23 January 2023).

30.	Bayan, F.P.; Cornetto, A.D.; Dunn, A.; Sauer, E. Brake Timing Measurements for a Tractor-Semitrailer Under Emergency Braking. *SAE Int. J. Commer. Veh.* **2010**, *2*, 245–255. [CrossRef]

31.	Ciępka, P.; Wolak, S. Czas narastania opóźnienia hamowania w motocyklach—Wyniki badań poligonowych. In Proceedings of the International Science-Technical Conference „Automotive Safety 2016", Kielce-Ameliówka, Poland, 22–24 February 2016; pp. 29–35. (In Polish)

32.	Stańczyk, L.T.; Jurecki, R.S.; Walczak, S.; Pieniążek, W. Analysis of the time of increase in forces applied to a brake pedal and braking deceleration determined during experimental testing of accident hazard situationson a testing track. *Autobusy Tech. Eksploat. Syst. Transp.* **2011**, *12*, 349–359. (In Polish)

33.	Lex, C. *Maximum Tire-Road Friction Coefficient Estimation*; Verlag der Technischen Universität: Graz, Austria, 2015. [CrossRef]

34.	Ma, B.; Xu, H. Vehicle Unsteady Dynamics Characteristics Based on Tire and Road Features. *Adv. Mech. Eng.* **2013**, *2013*, 153257. [CrossRef]

35.	Pokorski, J.; Sar, H.; Reński, A. Measurement system For Investigation of Tyre-Road Friction. In Proceedings of the International Scientific Conference MOSATT, Koszyce, Slovakia, 20–22 September 2011.

36.	Wu, J.; Wang, Y.S.; Su, B.L.; Liu, Q. Experimental and Numerical Studies on Tire Tread Block Friction Characteristics Based on a New Test Device. *Adv. Mater. Sci. Eng.* **2014**, *2014*, 816204. [CrossRef]

37.	Liu, X.; Wang, H.; Cao, Q.; Chen, J. Evaluation of Vehicle Braking Performance on Wet Pavement Surface using an Integrated Tire-Vehicle Modeling Approach. *Transp. Res. Rec. J. Transp. Res. Board* **2019**, *2673*, 295–307. [CrossRef]

38.	Zhang, Y.; Gao, J.; Li, Q. Experimental study on friction coefficients between tire tread rubber and ice. *AIP Adv.* **2018**, *8*, 075005. [CrossRef]

39.	Zuska, A.; Kurczynski, D.; Jackowski, J.T. Study of Loads Acting on the Load during the Sudden Braking of a Vehicle. *Appl. Sci.* **2023**, *13*, 1559. [CrossRef]

40.	Du, X.; Wang, G. Analysis of Operating Safety of Tractor-Trailer under Crosswind in Cold Mountainous Areas. *Appl. Sci.* **2022**, *12*, 12755. [CrossRef]

41.	MacIsaac, J.D. *Preliminary Findings of the Effect of Tire Inflation Pressure on the Peak and Slide Coefficients of Friction*; DOT HS 809428; National Highway Traffic Safety Administration: Washington, DC, USA, 2002.

42.	Schmeitz, A.J.C.; Nijmeijer, H.; Basselink, I. *Extending the Magic Formula and SWIFT Tyre Models for Inflation Pressure Changes*; Researchgate: Amsterdam, The Netherlands, 2005.

43.	Jin, H.; Zhou, M. On the road friction recognition based on the driving wheels deceleration. In Proceedings of the IEEE Conference and Expo Transportation Electrification Asia-Pacific (ITEC Asia-Pacific), Beijing, China, 31 August–3 September 2014; pp. 1–8. [CrossRef]

44.	Luty, W. *Transient Conditions of Tire Sideslip. Experimental and Model Research*; Publishing House of the Warsaw University of Technology: Warsaw, Poland, 2017. (In Polish)

45.	Zhu, Y.; Li, X.; Zhang, X.; Li, S.; Liu, Q.; Yuan, S. Research on Tire–Road Parameters Estimation Algorithm for Skid-Steered Wheeled Unmanned Ground Vehicle. *Machines* **2022**, *10*, 1015. [CrossRef]

46. Liu, X.; Al-Qadi, I.L. Development of a Simulated Three-Dimensional Truck Model to Predict Excess Fuel Consumption Resulting from Pavement Roughness. *Transp. Res. Rec.* **2021**, *2675*, 1444–1456. [CrossRef]

47. Lozia, Z. Application of Modelling and Simulation in Durability Tests of Vehicles and Their Components. *Energies* **2022**, *15*, 9398. [CrossRef]

48. Zhang, Q.; Su, C.; Zhou, Y.; Zhang, C.; Ding, J.; Wang, Y. Numerical Investigation on Handling Stability of a Heavy Tractor Semi-Trailer under Crosswind. *Appl. Sci.* **2020**, *10*, 3672. [CrossRef]

49. Westerhof, B.; Kalakos, D. *Heavy Vehicle Braking Using Friction Estimation for Controller Optimization*; KTH Royal Institute of Technology: Stockholm, Sweden, 2017.

50. Deng, J.; Ashley, D.; Guenther, D.; Heydinger, G. Adaptation of TruckSim Models to Simulate Experimental Heavy Truck Hard Braking Test Data Under Various Levels of Brake Disablement. In Proceedings of the SAE 2010 Commercial Vehicle Engineering Congress, Detroit, MI, USA, 5 October 2010. [CrossRef]

51. Andrew, J.D. *Braking of Road Vehicles*; Butterworth-Heinemann: Oxford, UK, 2014.

52. Rajamani, R. *Vehicle Dynamics and Control*; Springer Science & Business Media: New York, NY, USA, 2011. [CrossRef]

53. Svendenius, J.; Wittenmark, B. *Review of Wheel Modeling and Friction Estimation*; Technical Reports TFRT-7607; Department of Automatic Control, Lund Institute of Technology (LTH): Lund, Sweden, 2003.

54. Wang, T. Analysis on Tyre Wear. Modeling and Simulations. Degree Project in Vehicle Engineering. Master's Thesis, KTH Royal Institute of Technology, Stockholm, Sweden, 2017.

55. Selig, M.; Lorenz, B.; Henrichmoller, D.; Schmidt, K.; Ball, A.; Persson, B.N.J. Rubber Friction and Tire Dynamics: A Comparison of Theory with Experimental Data. *Tire Sci. Technol.* **2014**, *42*, 216–262. [CrossRef]

56. Gruber, P.; Sharp, R.S. Tyre Models for Vehicle Dynamics Analysis. In Proceedings of the 4th International Tyre Colloquium, University of Surrey, Guildford, UK, 20–21 April 2015.

57. Anupam, K.; Tang, T.; Kasbergen, C.; Scarpas, A.; Erkens, S. 3-D Thermomechanical Tire–Pavement Interaction Model for Evaluation of Pavement Skid Resistance. *Transp. Res. Rec.* **2021**, *2675*, 65–80. [CrossRef]

58. Tang, T.; Anupam, K.; Kasbergen, C.; Kogbara, R.; Scarpas, A.; Masad, E. Finite Element Studies of Skid Resistance under Hot Weather Condition. *Transp. Res. Rec.* **2018**, *2672*, 382–394. [CrossRef]

59. Xu, Z.; Lu, Y.; Chen, N.; Han, Y. Integrated Adhesion Coefficient Estimation of 3D Road Surfaces Based on Dimensionless Data-Driven Tire Model. *Machines* **2023**, *11*, 189. [CrossRef]

60. Pacejka, H.B. *Tire and Vehicle Dynamics*; Butterworth-Heinemann: Amsterdam, The Netherlands, 2012. [CrossRef]

61. Dugoff, H.; Fancher, P.S.; Segel, L. An analysis of tire traction properties and their influence on vehicle dynamic performance. In *SAE Technical Paper*; SAE International: Warrendale, PA, USA, 1970; p. 700377. [CrossRef]

62. Rill, G. An engineer's guess on tyre parameter made possible with TMeasy. In Proceedings of the 4th International Tyre Colloquium, University of Surrey, Surrey, UK, 20–21 April 2015.

63. Guo, K.; Lu, D. UniTire: Unified tire model for vehicle dynamic simulation. *Veh. Syst. Dyn.* **2007**, *45* (Suppl. S1), 79–99. [CrossRef]

64. Burckhardt, M. *Fahrwerktechnik: Radschlupf-Regelsysteme*; Vogel Buchverlag: Worzburg, Germany, 1993.

65. Kiencke, U.; Nielsen, L. *Automotive Control Systems: For Engine, Driveline, and Vehicle*, 2nd ed.; Springer: Berlin/Heidelberg, Germany, 2005.

66. Sider, A.; Amiri, A.; Hassan, M.K.; Mohd Radzi, M.A.; Toha, S.F. Mathematical design and analysis of anti-lock brake system for electric vehicle based on brake-by-wire technology. *Int. J. Electr. Hybrid Veh.* **2015**, *7*, 303–322. [CrossRef]

67. Communication Issued by Kraftfahrt-Bundesamt. Concerning a Confirmation of a Test Report regarding Annex 11 Appendix 2 Item 3.9.of ECE Regulation No. 13 for a Reference Axle/Brake, Kraftfahrt-Bundesamt, Germany. 2015. Available online: www.safholland.org (accessed on 16 November 2022).

68. Test Report for Applications of Annex 19, ECE Regulation No. 13, TÜV NORD Mobilität GmbH & Co. KG, Germany. 2007. Available online: www.wabco-customercentre.com (accessed on 16 November 2022).

69. Literature and Documents. Haldex. Available online: https://www.haldex.com/en/Europe/services-and-support/literaturedocuments/ (accessed on 16 November 2022).

70. Rely on S-ABA, Automatic Brake Adjuster. The Number 1 Worldwide, Haldex, Sweden. 2018. Available online: www.haldex.com (accessed on 16 November 2022).

71. Technical Card of Iveco Stralis MY2016, AS440S57T/FP LT XP. Iveco, Italy. 2017. Available online: www.iveco.com (accessed on 16 November 2022).

72. Box Semitrailer Kögel Type: SN24 P90/910 X-MAXX. Catalog Materials of Kögel, Burtenbach, Germany. 2020. Available online: www.koegel.com (accessed on 6 October 2022).

73. Dousti, M.; Baslamısli, S.C.; Onder, E.T.; Solmaz, S. Design of a multiple-model switching controller for ABS braking dynamics. *Trans. Inst. Meas. Control* **2015**, *37*, 582–595. [CrossRef]

74. Gontarz, A.; Czerwienko, D.; Pogorzelski, I.; Jurecki, L. Bezpieczeństwo Samochodów Pożarniczych w Czasie Jazdy i na Miejscu Akcj; Centrum Naukowo-Badawcze Ochrony Przeciwpożarowej (Scientific and Research Centre for Fire Protection National Research Institute): Józefów, Poland, 2012. Available online: https://depot.ceon.pl/handle/123456789/7749 (accessed on 11 October 2022). (In Polish)

75. Janczur, R.; Zawałeń, J. Dynamics of heavy duty vehicles motion after tyre blow out. *Paragraf Na Drodze* **2017**, *2017*, 115–127. (In Polish)

76. Pneumatic Brake Equipment for Trailer Vehicles. Product Catalogue. Europe. Edition 4, Wabco, Belgium. 2021. Available online: www.wabco-customercentre.com (accessed on 7 February 2023).
77. Zhang, Z.; Sun, N.; Chen, Y.; Ahmadian, M. Detailed Modeling of Pneumatic Braking in Long Combination Vehicles. *SAE Int. J. Commer. Veh.* **2021**, *14*, 245–258. [CrossRef]
78. Zhang, L.; Feng, S.; Shan, H.; Wang, G. Tractor-trailer-train braking time sequence detection based on monocular vision. *Adv. Mech. Eng.* **2021**, *13*, 16878140211067045. [CrossRef]
79. UNECE. Main Reports. Available online: https://unece.org/DAM/trans/main/wp29/wp29wgs/wp29grrf/grrfinf/49/49-inf0 2text-of-main-report.pdf (accessed on 7 February 2023).